

STUDY OF AURORAL DYNAMICS WITH COMBINED SPACECRAFT AND INCOHERENT SCATTER RADAR DATA

Jeffrey P. Thayer, Research Physicist
Odile de la Beaujardière, Principal Scientist
Jurgen Watermann, Research Physicist
Geoscience and Engineering Center

SRI Project 2781

Prepared for
National Aeronautics and Space Administration
Washington, D.C.

Contract NASW-4063

Approved:

James F. Vickrey, Director
Geoscience and Engineering Center

Murray J. Baron, Vice President
Advanced Development Division

1 SUMMARY OF RESULTS

The objectives of this project were to study the coupling between the ionosphere and the magnetosphere, and to understand how this coupling was affected by changes in the solar wind. The data used consisted of satellite measurements coordinated with Søndrestrom incoherent scatter radar observations. We focused our efforts on the study of temporal and spatial changes in the dayside auroral precipitation and electric field.

2 PROJECT HIGHLIGHTS

2.1 SMALL SPATIAL AND TEMPORAL CHANGES IN THE PRE-NOON AURORAL PRECIPITATION

On rare occasions, observations from the DMSP-F6 and -F8 spacecraft and the Søndrestrom incoherent scatter radar coincide in space. Such coincidence offers a unique opportunity to study temporal versus spatial variations on a small scale. We discuss data from one of those occasions, with observations made in the dawn sector in the presence of moderate auroral precipitation during a magnetically quiet period. The DMSP satellites measured vertical electron and ion flux and cross-track plasma drift while the radar measured the ionospheric electron density distribution and line-of-sight plasma velocities. We combine these data sets to construct a two-dimensional map of a possible auroral pattern above Søndrestrom, which is characterized by the following properties: No difference is seen between the gross precipitation patterns measured along the DMSP-F6 and -F8 trajectories (separated by 32 km in magnetic east-west direction and some 4 s in travel time in magnetic north-south direction), except that they are not exactly aligned with the L shells. However, F6 and F8 observed minor differences in the small-scale structures. More significant differences are found between small-scale features in the DMSP precipitation measurements and in radar observations of the E -region plasma density distribution. These measurements are separated by 74 km, equivalent to 2.4° , in magnetic longitude, and 0-40 s in time along the spacecraft trajectories (varying with magnetic latitude). Large-scale magnetospheric-ionospheric surfaces such as plasma flow reversal, poleward boundary of the keV ion and electron precipitation, and poleward boundary of E -region ionization, coincide. The combined data suggest that the plasma flow reversal delineates the polar cap boundary, that is, the boundary between precipitation characteristic for the plasma mantle and for the plasma sheet boundary layer.

2.2 CUSP OBSERVATIONS USING COMBINED VIKING, DMSP, AND SØNDRESTROM INCOHERENT SCATTER RADAR OBSERVATIONS

We have examined Søndrestrom incoherent scatter radar observations of ionospheric plasma density and temperature distributions and measurements of F -region ion drifts that were

made during a pre-noon pass of the DMSP-F7 satellite through the radar field of view. The spacecraft traversed a region of intense electron precipitation with a characteristic energy below approximately 200 eV. Particles with such low characteristic energies are believed to be directly or indirectly of magnetosheath origin. The precipitation region had a width of about 2° invariant latitude and covered the low-latitude boundary layer (LLBL), the cusp, and the equatorward section of the plasma mantle (PM). The co-rotating radar observed a patch of enhanced electron density and elevated electron temperature in the F2 region between about 10.5 and 12 magnetic local time in the same invariant latitude range where DMSP-F7 detected the soft-electron flux. The ion drift pattern, also obtained by radar, shows that it is unlikely that the plasma patch was produced by solar radiation and advected into the radar field of view. We suggest that the radar observed modifications of the ionospheric plasma distribution, which resulted from direct entry of magnetosheath electrons into the magnetosphere and down to ionospheric altitudes. Model calculations of the ionospheric response to the observed electron precipitation support our interpretation. The spectral characteristics of the electron flux in the LLBL, cusp, and equatorward section of the PM were in this case too similar to allow us to distinguish between them by using incoherent scatter radar measurements only.

3 SCIENTIFIC REPORTS

A paper describing the small spatial structure and temporal changes in auroral precipitation observed by the Søndrestrom radar and DMSP satellites has been published: Watermann, J., O. de la Beaujardière, and H.E. Spence, "Space-Time Structure of the Morning Aurora Inferred from Coincident DMSP-F6, -F8, and Søndrestrom Incoherent Scatter Radar Observations," *J. Atmos. Terr. Phys.*, 55, No. 14, pp. 1729-1739, 1993. (See Appendix A.)

A paper describing the detection of magnetosheathlike particle precipitation observed in the ionosphere has been published: Watermann, J., D. Lummerzheim, O. de la Beaujardière, P.T. Newell, and F.J. Rich, "Ionospheric Footprint of Magnetosheathlike Particle Precipitation Observed by an Incoherent Scatter Radar," *J. Geophys. Res.*, 99, No. A3, pp. 3855-3867, 1994. (See Appendix B.)

A paper describing combined radar and satellite observations of the cusp signature in the ionosphere has been accepted: Watermann, J., O. de la Beaujardière, D. Lummerzheim, J. Woch, P.T. Newell, T.A. Potemra, F.J. Rich, and M. Shapshak, "The Dynamic Cusp at Low Altitudes: A Case Study Utilizing Viking, DMSP-F7, and Søndrestrom Incoherent Scatter Radar Observations," *Annales Geophysicae*, in press, 1994. (See Appendix C.)

APPENDIX A

**Watermann, J., O. de la Beaujardière, and H.E. Spence,
“Space-Time Structure of the Morning Aurora Inferred
from Coincident DMSP-F6, -F8, and Søndrestrom
Incoherent Scatter Radar Observations,” J. Atmos. Terr.
Phys., 55, No. 14, pp. 1729-1739, 1993**

Space-time structure of the morning aurora inferred from coincident DMSP-F6, -F8, and Søndrestrøm incoherent scatter radar observations

J. WATERMANN,* O. DE LA BEAUJARDIÈRE* and H. E. SPENCE†

*Geoscience and Engineering Center, SRI International, 333 Ravenswood Avenue, Menlo Park, CA 94025, U.S.A.;

†The Aerospace Corporation, Space and Environment Technology Center, Los Angeles, CA 90009, U.S.A.

(Received in final form 26 May 1992; accepted 26 May 1992)

Abstract—On rare occasions, observations from the DMSP-F6 and -F8 spacecraft and the Søndrestrøm incoherent scatter radar coincide in space. Such coincidence offers a unique opportunity to study temporal vs spatial variations on a small scale. We discuss data from one of those occasions, with observations made in the dawn sector in the presence of moderate auroral precipitation during a magnetically quiet period. The DMSP satellites measured vertical electron and ion flux and cross-track plasma drift while the radar measured the ionospheric electron density distribution and line-of-sight plasma velocities. We combine these data sets to construct a two-dimensional map of a possible auroral pattern above Søndrestrøm. It is characterized by the following properties. No difference is seen between the gross precipitation patterns measured along the DMSP-F6 and -F8 trajectories (separated by 32 km in magnetic east–west direction and some 4 s in travel time in magnetic north–south direction), except that they are not exactly aligned with the L shells. However, F6 and F8 observed minor differences in the small-scale structures. More significant differences are found between small-scale features in the DMSP precipitation measurements and in radar observations of the E -region plasma density distribution. These measurements are separated by 74 km, equivalent to 2.4° , in magnetic longitude, and 0–40 s in time along the spacecraft trajectories (varying with magnetic latitude). Large-scale magnetospheric–ionospheric surfaces such as plasma flow reversal, poleward boundary of the keV ion and electron precipitation, and poleward boundary of E -region ionization, coincide. The combined data suggest that the plasma flow reversal delineates the polar cap boundary, that is, the boundary between precipitation characteristic for the plasma mantle and for the plasma sheet boundary layer.

1. INTRODUCTION

Coincident high-latitude ground-based and spaceborne measurements of ionospheric plasma parameters have been widely used in the past to study phenomena of magnetosphere–ionosphere coupling in more detail than would be possible from either one alone. Low-altitude spacecraft (orbiting below some 1000 km) are particularly convenient for this purpose. Field line mapping does not pose a problem, because an IGRF model is usually accurate enough and appropriate under various solar wind, magnetospheric, and ionospheric conditions. Auroral electron acceleration is often confined to altitudes above some 1000 km, for example, REIFF *et al.* (1988). Only occasionally significant acceleration is found below 800 km altitude, for example, RINNERT *et al.* (1986). Therefore, precipitation of energetic electrons (tens of eV to tens of keV), observed on low-altitude satellites, corresponds in most cases directly to ionospheric plasma density enhancements. Also, electric fields perpendicular to the magnetic field B_0 are approximately

the same at the spacecraft altitude and in the ionosphere, except for a magnetic field geometry factor.

The combination of coincident measurements from ground and space can enhance the space–time resolution of the observations and may allow mapping between magnetospheric boundaries and their ionospheric signatures, based on physically observable parameters (such as particle characteristics) instead of solely on magnetic field or electrostatic potential models. In this paper we discuss the exceptional case of having a triple set of such measurements, namely from two DMSP (Defense Meteorological Satellite Program) spacecraft (RICH *et al.*, 1985) and from the Søndrestrøm incoherent scatter radar (KELLY, 1983; WICKWAR *et al.*, 1984). Our study is not the first to combine Søndrestrøm radar observations and data from two low-altitude spacecraft. ROBINSON *et al.* (1984) examined coincident observations from the Søndrestrøm radar and from the Triad and NOAA-7 satellites. In a follow-up study, ROBINSON *et al.* (1988) analyzed coincident DMSP-F6, HILAT, and Søndrestrøm radar observations. In those two studies,

the satellites were widely spaced. The authors inferred the development of a large-scale auroral pattern, but small-scale variations could not be resolved. In this paper we examine data acquired simultaneously with two closely spaced low-altitude satellites and the Søndrestrøm radar.

We compare particle precipitation and plasma drift measurements from the SSJ/4 and SSIES instruments on DMSP-F6 and -F8 (RICH *et al.*, 1985) during a pass of the satellites in close formation over western Greenland with complementary ionospheric observations made with the Søndrestrøm incoherent scatter radar almost underneath the spacecraft trajectories. The combined data are used to determine the polar cap boundary, the distribution of the discrete aurora, and the plasma drift pattern in the dawn sector. The small temporal and spatial offsets between the three data sets yield information about the space-time structure of auroral patterns and the polar cap boundary with high resolution (a couple of seconds in time and a few tens of kilometers in magnetic longitude). They also allow us to compile a two-dimensional view of the auroral ionosphere over Søndrestrøm and its association with magnetospheric regions, even in the absence of auroral images.

2. OBSERVATIONS

The Søndrestrøm incoherent scatter radar is located at 67° geodetic latitude and 309° longitude. Its invariant latitude of 73.8° corresponds to $L = 12.8$, and the local contour of constant invariant latitude is rotated between 27° (at ground level) and 26° (at 1000 km altitude) counterclockwise from geographic east. These numbers are computed from the IGRF 1985 model, extrapolated to epoch 1990.3. During the event that we report here, the radar scanned the ionosphere with constant slew rate back and forth in a plane perpendicular to the local L shell. Each elevation scan took 4.5 min except the one preceding the DMSP passes which was stopped about 3 min prior to the satellite passes, before the antenna had reached lowest elevation, in order to synchronize the next scan with the satellite passes. The scan sequence was restarted with the antenna pointing southward at lowest elevation to achieve optimal coincidence with the polebound DMSP passes. The antenna motion was such that the antenna pointed along the field line when the spacecraft crossed the L shell through the radar location. To compensate for the weak radar signal (owing to the generally low ionospheric electron density) we used a fairly long integration time, 20 s corresponding to 30 km spatial integration at 120 km

overhead the radar. The electron density measurements above 120 km altitude were corrected with electron and ion temperatures obtained from fits to the measured spectra.

The DMSP-F6 and -F8 spacecraft move in nearly identical, Sun-synchronous circular orbits at 98° inclination, and they cross the equator near the dawn-dusk meridian. Because of their different altitudes (821 and 865 km, respectively), the spacecraft have slightly different velocities, with the effect that the lower F6 overtakes the higher F8 about once every eleven days. When passing over Søndrestrøm, the spacecraft trajectories happen to cross the contours of constant invariant latitude approximately perpendicularly. Although the F6 spacecraft was officially decommissioned after F8 began operation, simultaneous observations were made during a few periods of close approach between F6 and F8.

The F6 and F8 spacecraft measure charged particle precipitation in the energy range 30 eV–30 keV. Their electron and ion spectrometers are each divided into two channels, sensitive to particles below and above 1 keV, respectively. All four channels are scanned once per second through ten logarithmically spaced energy levels. The spectrometers are always pointing vertically upward, therefore pitch angle distributions cannot be determined. The DMSP-F8 driftmeter provides measurements of the vertical and horizontal cross-track plasma drift.

The sole event for which coincident data from the Søndrestrøm radar and both DMSP spacecraft are available took place on 4 April 1990, between 0801 and 0805 UT. The time corresponds to 6.2 h magnetic local time and 4.7 h solar local time at Søndre Strømfjord. At a solar zenith angle of 93° , the atmosphere was sunlit above 9 km altitude, therefore no auroral images are available to support our interpretation. The event occurred during an extended magnetically quiet period between two magnetic storms commencing 5 days before and 5 days after the event. During the event, the Kp index reached only 2+. IMF data are not available for this time interval. The AFGL ionosonde at Søndrestrøm did not detect F -layer echoes, only echoes from the E -layer with $f_0E \approx 4$ MHz, corresponding to a peak plasma density of $2 \cdot 10^{11} \text{ m}^{-3}$ (Buchau, private commun.). The ionosonde measurements are consistent with the incoherent scatter radar data which identified an E -region peak density of $1.5 \cdot 10^{11} \text{ m}^{-3}$. Despite the geomagnetic quiescence, auroral particle precipitation and small-scale thermal plasma density variations were observed.

The left-hand side of Fig. 1 gives an overview of the geographic configuration of the experiment. The time

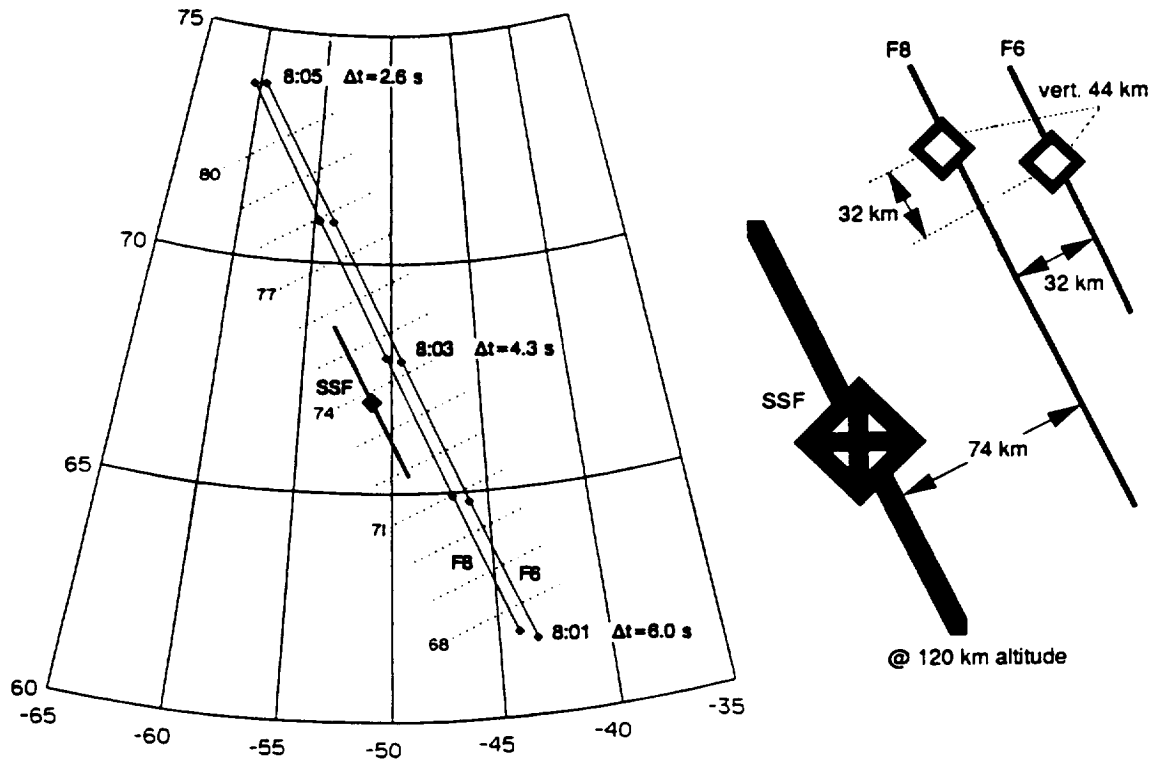


Fig. 1. Left : geographic latitude–longitude grid with the Søndrestrøm incoherent scatter radar (SSF) and its elevation scan trace (heavy), DMSP-F6 and -F8 trajectories, and invariant latitude contours (68–80°), all mapped to 120 km altitude. Δt = time difference between F6 and F8 on crossing the same invariant latitude. Right : enlarged central part of the grid including the radar location and the 0803 UT marks, showing the distances (mapped to 120 km altitude) between radar scan trace, F8 trajectory, and F6 trajectory.

difference Δt (seconds) denotes the delay between F8 and F6 on crossing the same L shell. The slightly higher F6 speed results in a shrinking lag, from $\Delta t = 6.0$ s at 0801 UT to $\Delta t = 2.6$ s at 0805 UT. On the right-hand side of Fig. 1 we have plotted an enlarged central section of the grid, showing the Søndrestrøm location with part of the scan trace and sections of the DMSP trajectories with the 0803 UT marks. At 120 km altitude, the horizontal distance along contours of constant invariant latitude is 74 km between radar scan plane and DMSP-F8 trajectory (2.4° in magnetic longitude) and 32 km between the two spacecraft trajectories (1° in magnetic longitude). The lag of $\Delta t = 4.3$ s corresponds to a latitudinal separation of 32 km (0.3°). The altitude distance between F6 and F8 was 44 km.

Figure 2 gives an overview of the DMSP-F8 particle precipitation and plasma drift measurements. We have plotted, from top to bottom, energy–time–intensity spectra of electrons and ions (particles $\text{cm}^{-2} \text{s}^{-1} \text{sr}^{-1} \text{eV}^{-1}$) and vertical and horizontal cross-track plasma drift components (m s^{-1}). Time runs from left to right, energy upward, the flux inten-

sity is color-coded (see the scaling bar on the right). The discontinuity close to the 1-keV energy level in both electron and ion spectra is artificial and caused by a mismatch between the low- and high-energy spectrometer channels at their transition point. The horizontal plasma drift is plotted in red; the westward (antisunward) velocity is positive and the eastward (sunward) negative. The vertical plasma velocity is plotted in blue, with positive meaning upward and negative downward. We have also marked the invariant latitudes (68–80°) corresponding to the interval of interest to our study. The dotted vertical line at 75.8° invariant indicates the poleward edge of the high-energy particle precipitation, which coincides with the plasma flow reversal from sunward to antisunward. Note, however, that the energetic particle precipitation boundary and the plasma flow reversal do not always coincide (DE LA BEAUJARDIÈRE *et al.*, 1993).

Figure 3 shows the horizontal plasma velocities in the radar scan plane (i.e. aligned with magnetic longitude) inferred from the radar scan made during the passes of the two DMSP spacecraft. Each velocity

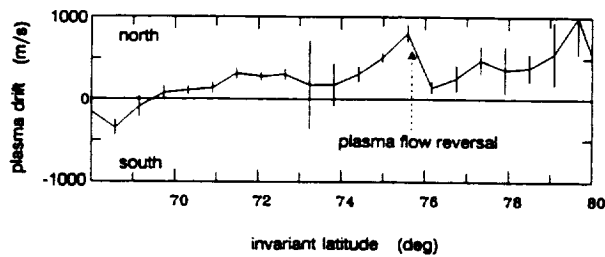


Fig. 3. Plasma drift in radar scan plane, perpendicular to the geomagnetic field and averaged over 0.6° invariant, from the radar elevation scan simultaneous with the DMSP passes (scan 2 in Fig. 6). Note the plasma flow reversal inferred from DMSP drift measurements.

estimate is obtained from several Doppler shift measurements made at various altitudes along a given magnetic field line. Between 73 and 74° invariant, where the radar beam is close to alignment with the magnetic field, the error bars become large. Otherwise the pattern is fairly stable with small error bars and shows northward velocities over most of the radar field-of-view. The velocity reaches a peak at 75.6° and drops abruptly towards the next bin at 76.2° invariant. Note that the flow reversal at 75.8° , inferred from Fig. 2 (lower panel), is located close to the peak of the northward velocity. Figure 3 seems to suggest that the reversal occurs poleward of the peak, but because the plasma velocities are averaged over 0.6° the uncertainty of the peak is $\pm 0.3^\circ$. When the velocities plotted in Fig. 3 are compared to those in Fig. 2 we notice that the east–west velocities (which exceed 1000 m s^{-1} over most of the 70 – 80° invariant latitude range and reach peaks of 2500 m s^{-1}) are significantly larger than the northward velocities except in the vicinity of the flow reversal and near 80° invariant.

By combining radar and spacecraft drift measurements (averaged over 0.6° invariant), we can construct the plasma flow pattern along the DMSP-F8 path. In so doing, we assume that the flow pattern is the same along the radar scan and the F8 trajectory (except for the altitude geometry factor) and remains constant over the few minutes it takes to complete the measurements. The result is displayed in Fig. 4 on the same latitude–longitude grid as used in Fig. 1. Following the trace from south to north, the flow orientation turns from magnetic southeastward to eastward (sunward) and rotates to westward (antisunward) in the vicinity of 76° . Poleward of the radar the velocity amplitudes are generally higher than equatorward of the radar. Such a pattern is seen very often in plasma convection measurements, see the average convection patterns (particularly the spring pattern) of DE LA BEAUJARDIÈRE *et al.* (1991).

Figure 5 shows the DMSP-F6 and -F8 measure-

ments of vertical electron and ion energy flux ($\text{eV cm}^{-2} \text{ s}^{-1} \text{ sr}^{-1} \text{ eV}^{-1}$), synchronized in invariant latitude. The range shown covers 69.5 – 79.8° invariant, as indicated by the tick marks. The central vertical thin line is only a window separator and without meaning for our discussion. In this figure, the flux parameter is different from that used in Fig. 2; there we have plotted the number flux, here the energy flux. It is obvious (and already known from earlier observations) that the F8 ion spectrometer was much noisier than the F6 instrument.

Between 71.7 and 75.8° invariant we find a structured precipitation pattern with electron energies up to 10 keV . One identifies five major bands of intense soft electron precipitation with the dominant part of the electron energy concentrated between 0.3 and 1.0 keV . The flux in the two outermost bands, around 71.8 and 74.9° invariant, is particularly intense over the energy range 30 eV – 1.2 keV . These bands are marked by open arrowheads and labeled intense low energy flux. Between them, at 74° invariant, we have placed a third open arrowhead labeled ‘radar arc’ whose meaning will become clear once we turn to Fig. 6. Here we only want to mention that no significant particle flux enhancement is associated with the ‘radar arc’.

A comparison between absolute flux intensities from F6 and F8 is hampered by aging of the particle spectrometers and by their different noise levels; therefore, we restrict our examination to the relative flux patterns. If we compare only the relative variations in the spectra from both satellites, we notice that the large-scale patterns are similar. F6 encounters the high energy cutoff 0.15° northward of F8; this distance corresponds to 2 s flight time or two spectral measurement frames, therefore this number bears 50% uncertainty. The invariant latitudes of some small-scale intensity enhancements and depressions also do not always coincide.

When examining the gross precipitation pattern we distinguish basically three regions.

(1) Poleward of 75.8° invariant we find the lowest flux intensities; in particular, the high-energy component is missing in all channels. This is characteristic of plasma mantle precipitation.

(2) The middle part, between 71.7° invariant and the high-energy flux cutoff at 75.8° invariant, shows moderately structured electron flux with significant small-scale variations below 1 keV . The observed ion fluxes reach high intensities at keV energies. We speculate that these particles are representative for the plasma sheet boundary layer.

(3) One notices a trend toward even higher electron

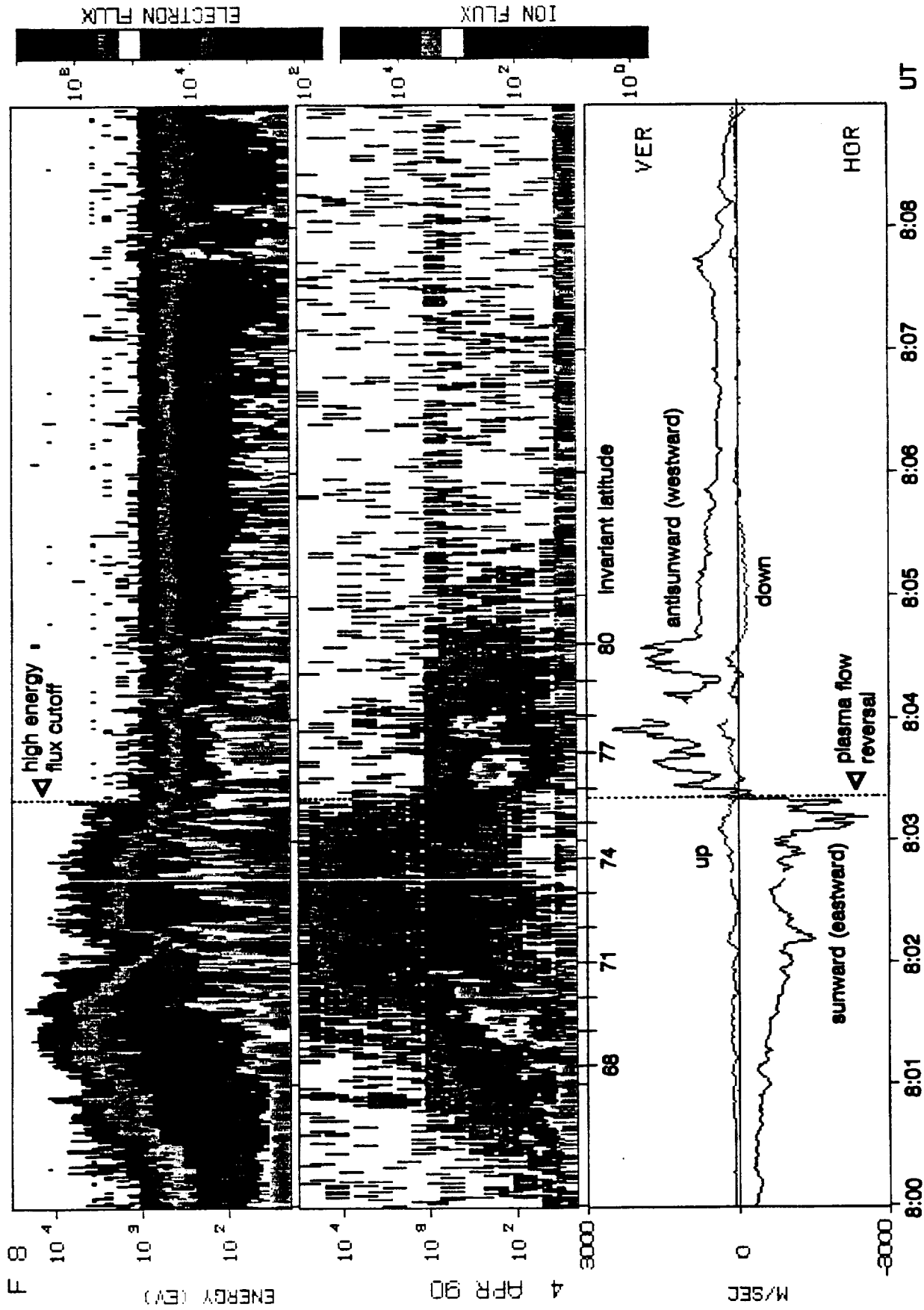


Fig. 2. DMSP-F8 measurements of the number flux of electrons (top panel) and ions (middle panel) and cross-track plasma drift (bottom panel). Universal Time and invariant latitude (at the 120 km footprint) are along the abscissa. High-energy flux cutoff and plasma flow reversal coincide.

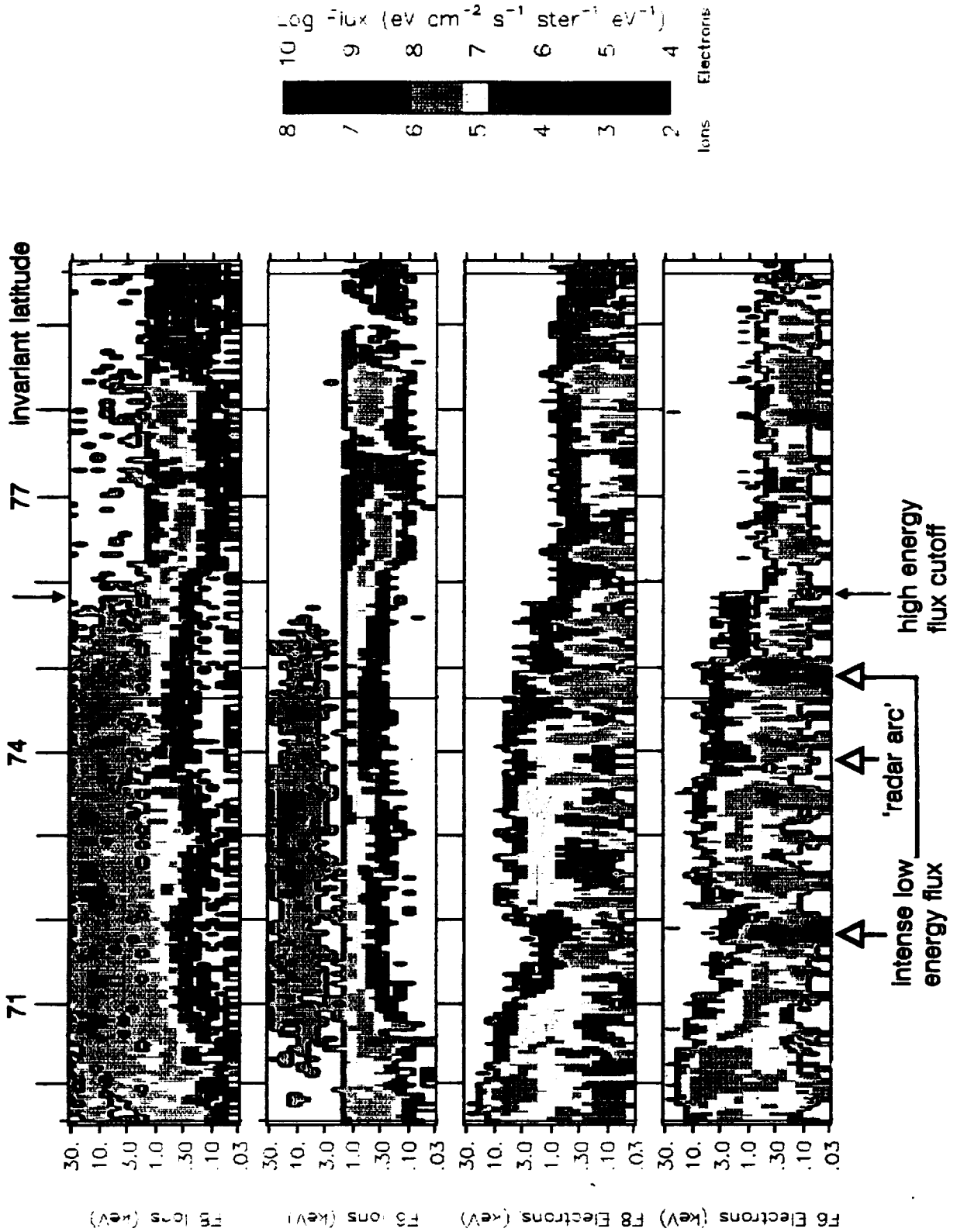


Fig. 5. Ion and electron energy flux measured onboard DMSP-F6 and -F8, synchronized in invariant latitude (tick marks on top and between the panels). From top to bottom: ions measured on F8, ions on F6, electrons on F8, and electrons on F6. The arrow labeled 'radar arc' refers to simultaneous radar observations of an auroral arc at this invariant latitude.

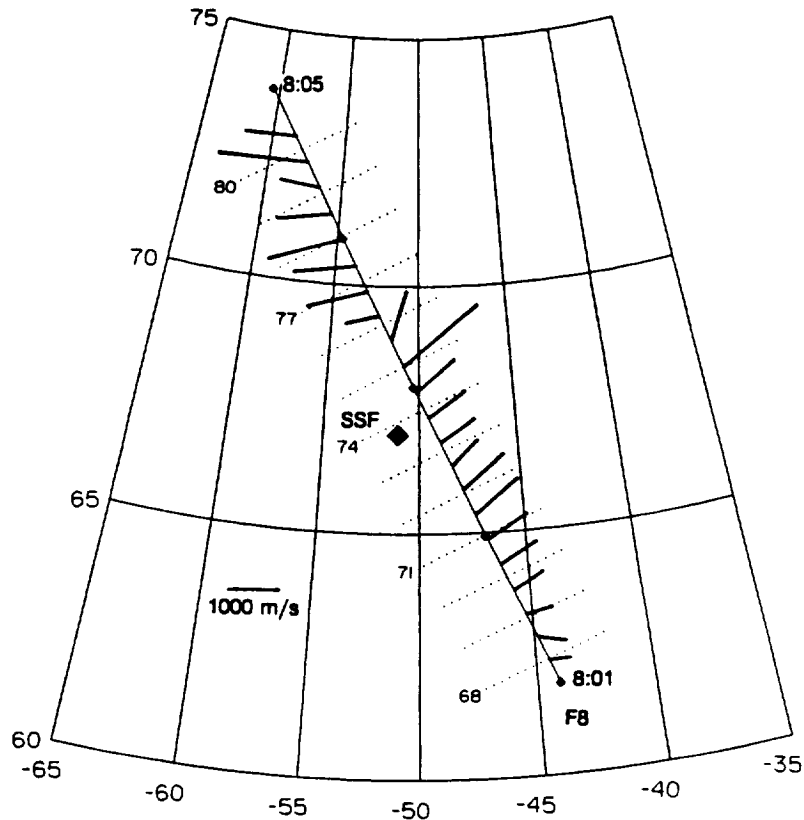


Fig. 4. Averaged plasma velocity vectors perpendicular to the geomagnetic field inferred from a combination of DMSP-F8 and radar drift measurements (Figs 2 and 3), plotted on the same grid as Fig. 1.

energies and less structured precipitation south of 71.7° invariant, accompanied by a drop-off in the high energy ion flux intensity. The diffuse character suggests precipitation of central plasma sheet particles.

Figure 6 shows the ionospheric electron density distributions measured by the incoherent scatter radar during four consecutive elevation scans, with the start times being 4.5 min apart from each other. Plotted are contours of equal electron density separated by 10^{10} m^{-3} . The scans were performed immediately before the DMSP passes (scan 1, antenna scanning from north to south), during the passes (scan 2, south to north), just after the passes (scan 3, north to south), and 9 min after the passes (scan 4, south to north). During scan 2, the radar beam was aligned with the geomagnetic field approximately at the same time the spacecraft crossed the L shell through Søndrestrøm. However, as time went on, the antenna motion lagged behind the spacecraft, such that some 80 s before the radar antenna had reached its lowest northward elevation the spacecraft field line, traced down to 120 km, passed the poleward edge of the E -region

radar field-of-view. Owing to the rotation of the Earth, the radar probed during scan 4 the same magnetic local time that the two satellites had sampled before. In other words, if one would replace the geographic grid of Fig. 1 by a geomagnetic grid, the trace of scan 4 would have been drawn between the F6 and F8 trajectories.

We have included in Fig. 6 dotted lines which correspond to the arrows plotted in Fig. 5. The arrow that was labeled 'radar arc' in Fig. 5 points to a localized region of enhanced plasma density in the upper E -layer seen during scan 2. The radar observations of this arc were made within a few seconds around the time the DMSP spacecraft measured low flux intensity at the same invariant latitude but offset by 2.4° in magnetic longitude. During scan 4, the radar detected an E -region plasma density enhancement (an auroral arc) at 74.3° invariant. This is close in latitude to the 'radar arc' of scan 2, but this arc is newly generated because enhanced plasma density at this latitude is not seen during the radar scan 3. The southernmost region of intense low-energy electron flux, at 71.7° invariant in Fig. 5, is near the equatorward edge of

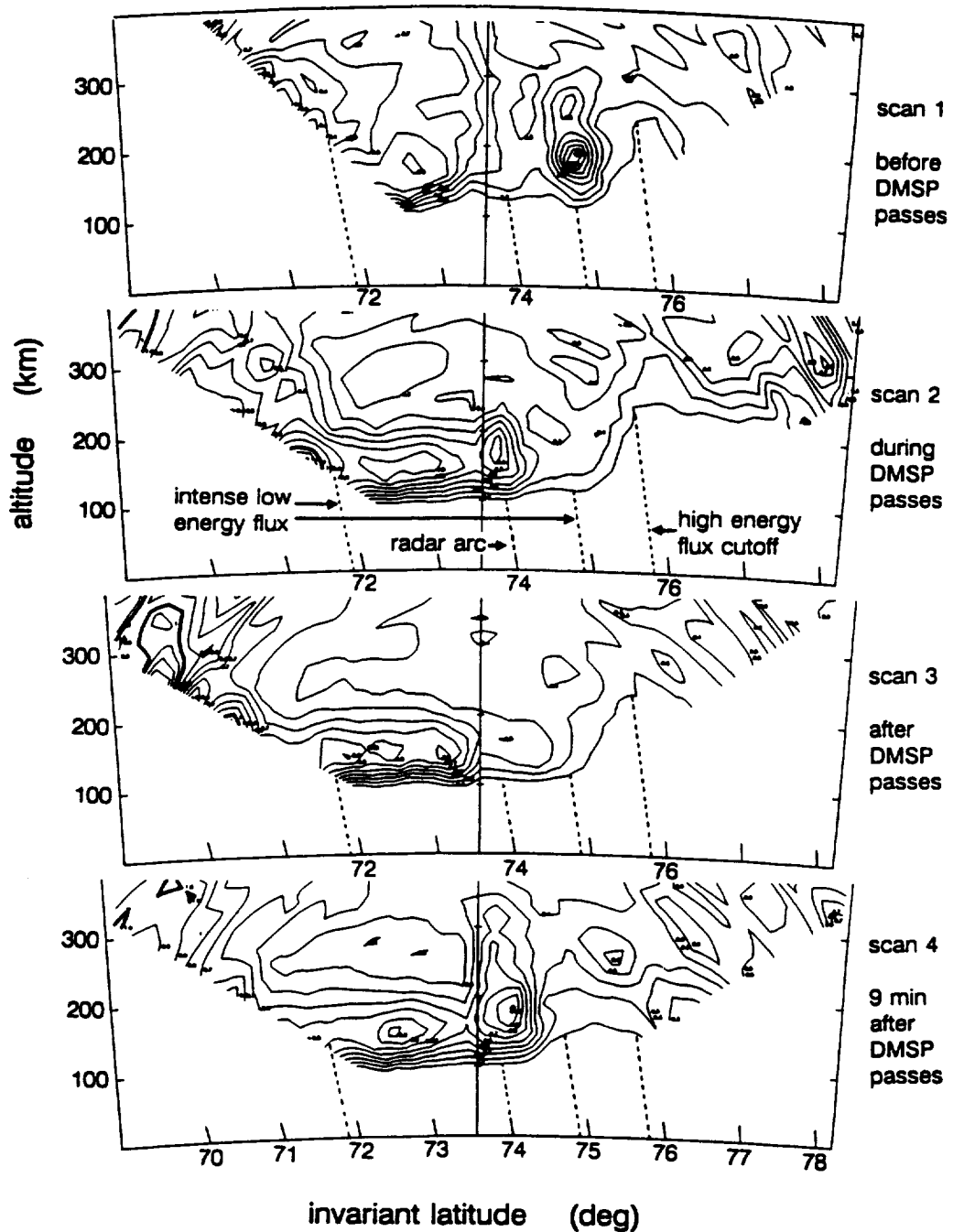


Fig. 6. Ionospheric raw plasma density profiles obtained from four consecutive radar elevation scans separated by 4.5 min. Contours of constant plasma density in steps of 10^{10} m^{-3} , beginning with $2 \cdot 10^{10} \text{ m}^{-3}$. Dotted lines correspond to the arrows in Fig. 5.

the *E*-region radar field-of-view, so that no conclusive statement about the corresponding ionospheric plasma density can be made. It appears that equatorward of 73.6° the *E*-region plasma density is enhanced in all four radar scans. This is in accordance with ionization from the 1–10 keV electron flux seen

in Fig. 5. The interval of intense low-energy flux at 74.9° invariant has no obvious counterpart in the ionospheric plasma density distribution seen during scan 2. This latitude was illuminated by the radar about 40 s after the spacecraft had passed across it. Instead, enhanced electron density is seen right at this

point during radar scan 1. The poleward boundary of the high-energy precipitation, labeled high-energy flux cutoff in Figs 4 and 5, coincides with the poleward edge of measurable *E*-region ionization during the first three scans and seems to have moved poleward by the time scan 4 was performed.

3. DISCUSSION AND CONCLUSIONS

A synoptic examination of the Søndrestrøm incoherent scatter radar and DMSP satellite observations leaves us with a situation that can be summarized as follows. We find coincidence between the reversal of the plasma flow from sunward to antisunward, the poleward boundary of energetic (>1 keV) electron and ion precipitation, and the poleward boundary of *E*-region ionization in excess of some $2 \cdot 10^{10} \text{ m}^{-3}$. The latter remained stable over the time of the first three radar scans shown in Fig. 4 (some 9 min), but varied during the preceding (not shown) and succeeding scans. We notice that the gross features of the particle precipitation observed on F6 and F8, with scale sizes exceeding one degree invariant, are similar though slightly misaligned with contours of constant invariant latitude. The small-scale structures (scale size of a fraction of one degree invariant) differ considerably more. Radar measurements made almost simultaneously with the DMSP passes show only partial coincidence between the *E*-region plasma density enhancements and the highest intensities in electron precipitation. For instance, the high *E*-region plasma density just poleward of the radar location (labeled 'radar arc') corresponds to electron flux of low intensity, and the intense soft electron flux near 74.9° invariant corresponds to low *E*-region plasma density a couple of seconds after the DMSP pass, but to high plasma density a few minutes before the pass. Between 72 and 75.8° a significant part of the electron energy flux observed on DMSP is carried by 1–10 keV electrons. More specifically, between 72.2 and 73.6° invariant a weak inverted-V structure can be identified in the F6 data, and within it slightly more of the electron energy flux is carried by the higher energy particles than is poleward of this structure. The F8 electron spectra do not show an inverted-V signature similar to that in the F6 data. The region equatorward of 73.6° invariant is in all radar scans characterized by enhanced plasma density in the lower *E*-region.

This situation suggests the following conclusions.

(1) The separation between the two DMSP spacecraft of 1° in magnetic longitude (32 km) and 4–5 s in time was too small to leave room for a significant change in the gross pattern of auroral precipitation.

The electron spectra show that the polar cap boundary, identified by the high-energy flux cutoff, was either not aligned with the *L* shell or has moved several kilometers poleward during the 4 s delay between the DMSP-F6 and -F8 measurements. A short-time fluctuation consistent with such a motion may indeed have occurred. But a steady poleward motion of the polar cap boundary over several minutes is not consistent with the radar data. The *E*-region reacts instantaneously on keV electron precipitation, and a steady motion with 1 km s^{-1} would be seen in the radar data as a shift of the *E*-region poleward boundary by several degrees invariant between scan 1 and scan 3.

(2) The 2.4° (74 km) separation between DMSP-F8 trajectory and the radar scan plane and the time lag between radar and spacecraft measurements (from 0 s at 74° to 40 s at 76° invariant) were large enough to result in significant differences between electron precipitation pattern and *E*-region plasma density enhancements.

These findings may be compared to results from Dynamics Explorer measurements obtained by THIEMAN and HOFFMAN (1985), who examined the correlation between inverted-V events observed on DE-1 and DE-2 during close-proximity passes. They found correlated events at approximately constant invariant latitude up to 18 min apart, but also the disappearance of some inverted Vs within one minute. Although the authors did not investigate the correlation span in magnetic longitude, they assumed that inverted Vs extend over a broad range of local times. Our observations in the dawn sector indicate that correlation of auroral forms including inverted Vs can cease on much smaller scales, a couple of seconds in time and 1° in magnetic longitude.

Ultraviolet auroral images from the Viking spacecraft show quite often bright spots in the dayside auroral oval, resembling beads on a string (LUI *et al.*, 1989). These bright spots were seen mostly in the afternoon sector during substorms, but at times appeared in the morning sector and during non-substorm intervals. The authors report lifetimes down to one image frame (1 min) and spatial dimensions of 50–200 km. These numbers are consistent with our data.

A possible interpretation of the observations is sketched in Fig. 7. This figure is drawn on the grid used in Fig. 1. Here we use magnetic longitude as a measure of magnetic local time. Proceeding to the left in Fig. 7 means looking at earlier and proceeding to the right means looking at later magnetic local times. Radar observations made during scan 1 will show up on the left of the diamond which marks the radar

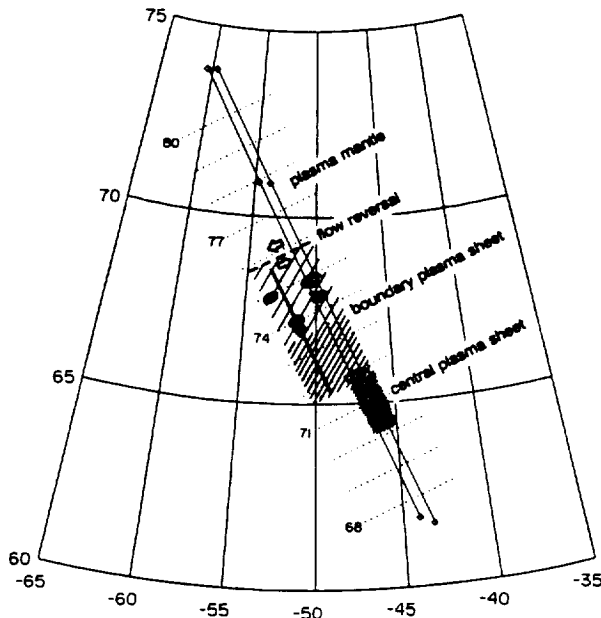


Fig. 7. A possible interpretation of the combined radar and spacecraft observations plotted on the grid used in Fig. 1. Footprints of magnetospheric regions as suggested by the DMSP and radar observations, including plasma mantle, boundary plasma sheet, and central plasma sheet. See text for details.

location, measurements during scan 2 in the vicinity of the diamond, and data from scans 3 and 4 to the right of the diamond.

We have marked by open arrows the drift orientations on both sides of the flow reversal. On the poleward side, very little precipitation was observed by the spacecraft and no significant *E*-region ionization was detected by the radar over some 15 min (equivalent to 4° magnetic longitude). This is indicative of the plasma mantle. Equatorward of the reversal, down to 71.7° invariant, we find a region where the spacecraft observed structured energetic particle precipitation (discrete arcs). The poleward section of this region is lightly hatched and corresponds to radar observations of structured, temporally variable *E*-region ionization. The equatorward section, south of 73.6° invariant, is more densely hatched to indicate the higher *E*-region plasma density throughout the four radar scans which coincides with the electron flux component of higher maximum energy. The poleward boundary of this region shifts slightly from one radar scan to the next, which is not reproduced in Fig. 7. We suggest that the particle flux between 71.7 and 75.8° invariant is characteristic of the plasma sheet boundary layer.

The localized band of enhanced particle flux recorded by DMSP near 74.9° invariant is indicated by

small concentric ovals. This spot does not extend to the left of the satellite trajectories because no arc was observed by the radar. A dark spot is placed to the left of the radar scan trace at 75° invariant. It corresponds to the region of enhanced *E*-region plasma density seen by the radar in scan 1, which is indicative of intense electron precipitation. The dark spot just north of the radar location indicates the 'radar arc', seen in scan 2 but not in scans 1 and 3 and in the particle precipitation patterns. A nearby arc appears in scan 4, 9 min later, at 74.3° invariant and is indicated by another dark spot. Finally, the intense electron flux observed by DMSP at 71.8° invariant is marked by concentric ovals across the trajectories. The radar data seem to indicate an auroral arc between 71 and 72° invariant during scan 2. But the structure appears at the equatorward edge of the *E*-region radar field-of-view, and the radar data are not conclusive. Therefore we did not extend that arc to the radar scan trace. We have examined several coincident DMSP-F7 and Søndrestrom radar measurements which seem to indicate that a localized *E*-region plasma density enhancement frequently coincides with the poleward edge of diffuse electron precipitation.

Finally, south of 71° invariant, beyond the equatorward edge of the *E*-region radar field-of-view, we have noticed high-energy electron precipitation with energy increasing even more toward the south (see Figs 2 and 5). We have characterized this region by a densely hatched pattern in Fig. 7 and labeled it the central plasma sheet.

Although Fig. 7 provides a possible view of the auroral structure during some 15 min of radar and DMSP observations, we emphasize that our interpretation is not the only one possible. We have assumed that the pattern is static in an invariant latitude-magnetic local time frame. To assume temporal stability is probably correct for the location of the poleward boundary of particle precipitation and associated *E*-region ionization. However, it is apparently not correct with respect to details of the discrete aurora, as the comparison between DMSP particle and radar data demonstrates. The various spots, which indicate discrete auroral arcs, are most likely a result of a combination of temporal and spatial variation. This is best demonstrated by comparing the DMSP electron precipitation measurements with the radar scans 2 and 4. The 'radar arc' at 74° invariant in scan 2 appears to be coincident with weak electron precipitation at the same Universal Time but earlier magnetic local time, and the arc at 74.3° invariant seen in scan 4 corresponds to weak electron precipitation at the same magnetic local time but later Universal Time.

In concluding we emphasize that in the event discussed, the precipitation fine structure exhibits some differences between the flux measurements made by the two closely-spaced satellites, but the gross precipitation patterns appear to be similar. The spatial and temporal separation of 74 km (2.4° magnetic longitude) and 0–40 s between radar and spacecraft measurements was large enough that patterns of the discrete aurora appear to be significantly different between radar and satellite observations.

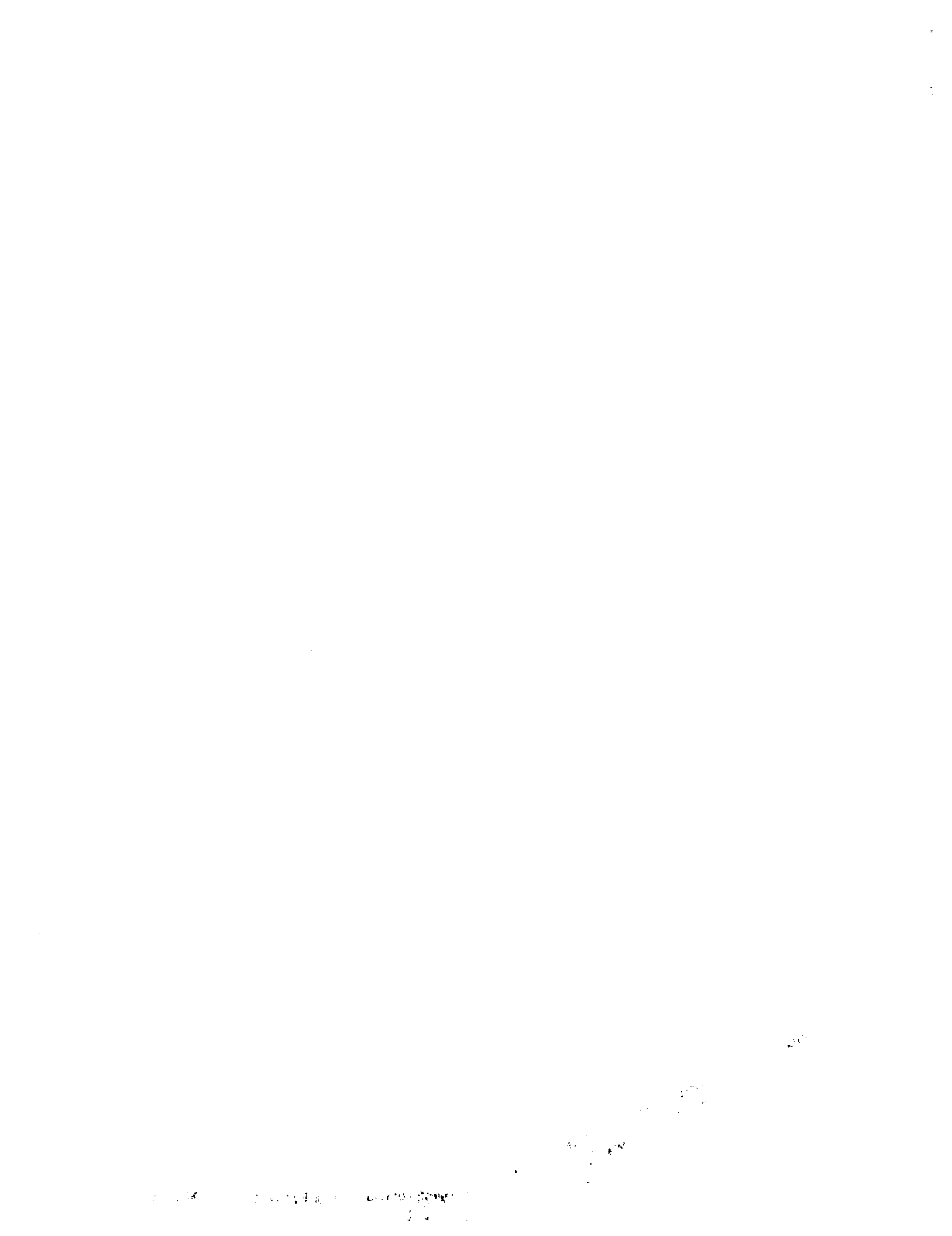
Acknowledgements—The work performed at SRI International was funded through the NSF–Søndrestrøm Cooperative Agreement ATM-8822560, NSF grant ATM-9017725, and NASA contracts NASW-4399 and NASW-4603. The work performed at The Aerospace Corporation was supported by the U.S. Air Force System Command's Space System Division under contract F04701-88-C-0089. We thank D. Hardy and F. J. Rich of Phillips Laboratory and R. A. Heelis of University of Texas at Dallas for providing data from the SSJ/4 particle spectrometers and the SSIES thermal plasma experiment flown on the DMSP spacecraft.

REFERENCES

- | | | |
|---|------|---|
| DE LA BEAUJARDIÈRE O., ALCAYDE D.,
FONTANARI J. and LEGER C. | 1991 | Seasonal dependence of high-latitude electric fields. <i>J. geophys. Res.</i> 96 , 5723. |
| DE LA BEAUJARDIÈRE O., WATERMANN J., NEWELL P.
and RICH F. | 1993 | Relationship between Birkeland current regions, particle precipitation, and electric fields. <i>J. geophys. Res.</i> (in press). |
| LUI A. T. Y., VENKATESAN D. and MURPHREE J. S. | 1989 | Auroral bright spots on the dayside oval. <i>J. geophys. Res.</i> 94 , 5515. |
| KELLY J. D. | 1983 | Søndrestrøm radar—initial results. <i>Geophys. Res. Lett.</i> 10 , 1112. |
| REIFF P. H., COLLIN H. L., CRAVEN J. D.,
BURCH J. L., WINNINGHAM J. D., SHELLEY E. G.,
FRANK L. A. and FRIEDMAN M. A. | 1988 | Determination of auroral electrostatic potentials using high- and low-altitude particle distributions. <i>J. geophys. Res.</i> 93 , 7441. |
| RICH F. J., HARDY D. A. and GUSSENHOVEN M. S. | 1985 | Enhanced ionosphere–magnetosphere data from the DMSP satellites. <i>Eos</i> 66 , 513. |
| RINNERT K., KOHL H., SCHLEGEL K. and
WILHELM K. | 1986 | Electric field configuration and plasma parameters in the vicinity of a faint auroral arc. <i>J. atmos. terr. Phys.</i> 48 , 867. |
| ROBINSON R. M., EVANS D. S., POTEMRA T. A. and
KELLY J. D. | 1984 | Radar and satellite measurements of an <i>F</i> -region ionization enhancement in the post-noon sector. <i>Geophys. Res. Lett.</i> 11 , 899. |
| ROBINSON R. M., VONDRAK R. R., HARDY D.,
GUSSENHOVEN M. S., POTEMRA T. A. and
BYTHROW P. F. | 1988 | Electrodynamics of very high latitude arcs in the morning sector auroral zone. <i>J. geophys. Res.</i> 93 , 913. |
| THIEMAN J. R. and HOFFMAN R. A. | 1985 | Determination of inverted-V stability from Dynamics Explorer satellite data. <i>J. geophys. Res.</i> 90 , 3511. |
| WICKWAR V. B., KELLY J. D.,
DE LA BEAUJARDIÈRE O., LEGER C. A.,
STEENSTRUP F. and DAWSON C. H. | 1984 | Søndrestrøm overview. <i>Geophys. Res. Lett.</i> 11 , 883. |

APPENDIX B

**Watermann, J., D. Lummerzheim, O. de la Beaujardière,
P.T. Newell, and F.J. Rich, "Ionospheric Footprint of
Magnetosheathlike Particle Precipitation Observed by an
Incoherent Scatter Radar," J. Geophys. Res., 99, No. A3,
pp. 3855-3867, 1994**



APPENDIX C

**Watermann, J., O. de la Beaujardière, D. Lummerzheim,
J. Woch, P.T. Newell, T.A. Potemra, F.J. Rich, and
M. Shapshak, "The Dynamic Cusp at Low Altitudes:
A Case Study Utilizing Viking, DMSP-F7, and
Søndrestrom Incoherent Scatter Radar Observations,"
Annales Geophysicae, in press, 1994**

A reprint of this paper was not available for inclusion in this report at the time of submission. Three copies will be sent under separate cover upon receipt from publisher.



Report Documentation Page

1. Report No.	2. Government Accession No.	3. Recipient's Catalog No.	
4. Title and Subtitle Study of Auroral Dynamics with Combined Spacecraft and Incoherent-Scatter Radar Data		5. Report Date September 1994	
		6. Performing Organization Code	
7. Author(s) Jeffrey P. Thayer, Odile de la Beaujardière, Jürgen Watermann		8. Performing Organization Report No. Final Report, SRI Project 2781	
		10. Work Unit No.	
9. Performing Organization Name and Address SRI International 333 Ravenswood Avenue Menlo Park, California 94025-3493		11. Contract or Grant No. NASW-4063	
		13. Type of Report and Period Covered Final Report	
12. Sponsoring Agency Name and Address		14. Sponsoring Agency Code	
		15. Supplementary Notes	
16. Abstract The objectives of this project were to study the coupling between the ionosphere and the magnetosphere, and to understand how this coupling was affected by changes in the solar wind. The data used consisted of satellite measurements coordinated with Sondrestrom incoherent scatter radar observations. We focused our efforts on the study of temporal and spatial changes in the dayside auroral precipitation and electric field.			
17. Key Words [Suggested by Author(s)] magnetosphere-ionosphere interaction magnetosphere particle fluxes field-aligned currents		18. Distribution Statement	
19. Security Classif. (of this report) UNCLASSIFIED	20. Security Classif. (of this page) UNCLASSIFIED	21. No. of pages	22. Price

Ionospheric footprint of magnetosheathlike particle precipitation observed by an incoherent scatter radar

Jurgen Watermann,^{1,2} Dirk Lummerzheim,³ Odile de la Beaujardière,¹ Patrick T. Newell,⁴ and Frederic J. Rich⁵

Abstract. We have examined Sondrestrom incoherent scatter radar observations of ionospheric plasma density and temperature distributions and measurements of *F* region ion drifts that were made during a prenoon pass of the DMSP-F7 satellite through the radar field of view. The spacecraft traversed a region of intense electron precipitation with a characteristic energy below approximately 200 eV. Particles with such low characteristic energies are believed to be directly or indirectly of magnetosheath origin. The precipitation region had a width of about 2° invariant latitude and covered the low-latitude boundary layer (LLBL), the cusp, and the equatorward section of the plasma mantle (PM). The corotating radar observed a patch of enhanced electron density and elevated electron temperature in the *F2* region between about 10.5 and 12 magnetic local time in the same invariant latitude range where DMSP-F7 detected the soft-electron flux. The ion drift pattern, also obtained by radar, shows that it is unlikely that the plasma patch was produced by solar radiation and advected into the radar field of view. We suggest that the radar observed modifications of the ionospheric plasma distribution, which resulted from direct entry of magnetosheath electrons into the magnetosphere and down to ionospheric altitudes. Model calculations of the ionospheric response to the observed electron precipitation support our interpretation. The spectral characteristics of the electron flux in the LLBL, cusp, and equatorward section of the PM were in this case too similar to allow to distinguish between them by using incoherent scatter radar measurements only.

Introduction

Certain magnetopause boundary regions, including the cusps, the low-latitude boundary layer (LLBL) and the plasma mantle (PM), play an important role in the transfer of plasma and magnetic flux from the solar wind into the magnetosphere. The cusps are relatively small regions in the high-latitude noon sectors of both hemispheres. In closed magnetosphere models, these cusps connect the magnetopause neutral points with singular points in the ionosphere. In open magnetosphere models the magnetopause is interrupted in the exterior cusp, and the cusps form a funnel through which magnetosheath plasma has the most direct access

to the ionosphere [cf. *Haerendel et al.*, 1978; *Kremser and Lundin*, 1990]. This terminology concurs with the conceptual cusp definition proposed by *Newell and Meng* [1988].

Owing to the large magnetopause surface and the relative scarcity of spacecraft observations in the magnetospheric boundary regions, in situ observations of the boundary layers are not often available. To study boundary layer processes, it is helpful to use indirect measurements from low-altitude spacecraft and ground-based instruments. Low-altitude magnetospheric and ionospheric observations take advantage of the fact that the magnetospheric boundary layers map to a relatively small area in the high-latitude ionosphere (see, for instance, Figure 3 of *Lundin* [1991] for a graphic representation of statistical magnetospheric boundary layer footprints).

The concept of categorizing magnetospheric boundary regions by means of charged-particle precipitation characteristics is only one of several possibilities, although probably the most widely used. Other definitions are based on properties of various other physical observables. These include visible auroral emissions [*Sandholt et al.*, 1985; *Sivjee*, 1985; *McEwen*, 1985], coherent HF radar backscatter [*Baker et al.*, 1990], magnetic pulsations [*Engbreton et al.*, 1986; *Olson*, 1986], the correlation between optical emissions and geomag-

¹Geoscience and Engineering Center, SRI International, Menlo Park, CA

²Now at: NATO SACLANT Undersea Research Centre, Viale San Bartolomeo 400, I-19138 San Bartolomeo, La Spezia, Italy.

³Geophysical Institute, University of Alaska, Fairbanks, AK

⁴Applied Physics Laboratory, Johns Hopkins University, Laurel, MD

⁵Phillips Laboratory, Hanscom Air Force Base, Bedford, MA

Copyright 1994 by the American Geophysical Union.

Paper number 93JA01995.
0148-0227/94/93JA-01995\$05.00

netic pulsations [McHarg and Olson, 1992], VLF signal characteristics and ionospheric absorption of cosmic noise [Engebretson et al., 1990], and field-aligned currents (consider, for instance, the current systems traditionally named cusp current and mantle current, e.g., Bythrow et al. [1988]).

Our paper deals with the identification of magnetospheric boundary regions from ground-based incoherent scatter radar observations. These boundary regions, which include the cusp, the LLBL, and the PM, are identified from the characteristics of particle precipitation observed on the DMSP-F7 spacecraft. We then analyze radar observations of the ionosphere made during several hours around the relevant satellite pass through the radar field of view to determine the properties of the ionospheric plasma within the region of magnetosheath-like soft electron precipitation. The characteristic energy of the electron flux is below some 200 eV, and we consider this flux typical for magnetosheathlike plasma precipitation. Using an auroral model, we find that the density and temperature variations of the ambient plasma, as observed by the radar, indeed concur with model predictions of the ionospheric response to the observed electron precipitation.

To our knowledge, no work has been published except for the papers by Kofman and Wickwar [1984] and Wickwar and Kofman [1984] that addresses specifically the ionospheric signature of soft-electron precipitation near local noon, observed with an incoherent scatter radar. Both papers suggest particle precipitation as a possible source for the measured increases of thermal electron density and temperature in the ionospheric *F* region. However, no satellite observations of particle precipitation were available to confirm the suggestion.

Observations

We will focus our discussion on satellite and radar data taken on 28 June 1984 in the dayside ionosphere, during a 68-hour incoherent scatter World Day experiment. The Sondrestrom incoherent scatter radar [Kelly, 1983], which participated in this experiment, is located at 67° latitude and 309° longitude on the west coast of Greenland; the *E* region at 120-km altitude above the radar site is intersected by the 74° invariant latitude contour. During the experiment, the radar performed repetitive antenna steering cycles, which included an elevation scan followed by multiple fixed positions. In the elevation scans, the antenna moved with constant angular speed of 0.4°/s in a vertical plane perpendicular to the local *L* shell; a complete scan took 5 min. The elevation scans yield images of the plasma density and temperature distributions in the scan plane, in an altitude versus invariant latitude frame. During the multiposition part of the radar cycle, the antenna was kept fixed at each of eleven different positions for times varying between 30 and 120 s, depending on the antenna elevation. In one of those positions, the radar beam was field-aligned; in three of the five pairs, the antenna was pointed poleward at 30°, 50°, and 65° ele-

vation; in the remaining two pairs, it was directed equatorward at 50° and 30° elevation. A pair consists of two antenna positions (at a fixed elevation), one directed a few degrees to the west and the other a similar amount to the east of the magnetic meridian through Sondrestrom (which is found 27° counterclockwise from geographic north). The multiposition measurements yield estimates of the plasma convection pattern over a wide range of invariant latitudes, provided the plasma drift on a given *L* shell is uniform within the radar field of view.

The DMSP-F7 satellite moved poleward through the Sondrestrom radar field of view and, at 1124 UT, its *E* region footprint crossed 74° invariant latitude some 130 km west of Sondrestrom. We use electron and ion energy spectra measured aboard this satellite as our reference for determining the footprints of magnetospheric regions. The DMSP particle spectrometers [Hardy et al., 1984] sample the electron and ion precipitation with 1-s resolution (equivalent to 7.4-km flight distance). Such a resolution is much better than the radar integration time of 20 s in this particular experiment, which is equivalent to 35-km integration distance at 280-km altitude. Because of this limitation, it is not possible to identify the boundaries of magnetospheric regions from radar observations with the same resolution as from spacecraft observations.

Plate 1 shows electron and ion spectrograms measured by DMSP-F7 between 1222 and 1226 UT. Plate 1 contains four panels with common UT and InvLat (invariant latitude) abscissa. All scales used along the ordinate are logarithmic. The upper panel shows the total energy flux JE of electrons (black) and ions (orange) in $\text{eV cm}^{-2} \text{s}^{-1} \text{sr}^{-1}$, the plotted ranges are offset by one order of magnitude (electrons span the range 10^9 – 10^{13} , ions 10^8 – 10^{12}). The second panel shows the average energy E in eV of the electron and ion fluxes. The third panel shows the electron energy spectrum in $\text{eV cm}^{-2} \text{s}^{-1} \text{sr}^{-1} \text{eV}^{-1}$, the intensity is color-coded according to the color bar at the right. The bottom panel shows the ion-energy spectrum in the same units. Note that the ordinate in this panel is inverted and that the intensities of the electron and ion precipitation displayed in the same color differ by 2 orders of magnitude. At the top of the plate, we have indicated the magnetospheric regions as identified from particle characteristics, based on the criteria developed by Newell and Meng [1988, 1989]. DMSP-F7 first crossed a region of precipitating particles characteristic for the central plasma sheet (CPS); the spacecraft then encountered the low-altitude footprint of the LLBL, followed by the cusp and the PM. The precipitation poleward of the PM could not unambiguously be associated with a particular magnetospheric source region. Its spectral properties resemble those of PM precipitation; however, the precipitation is of unusually high intensity. Finally, the spacecraft entered the polar rain (PR) region. The cusp proper was detected around 1224 UT, near 10 MLT (magnetic local time), between 73.8° and 74.3° invariant latitude, and was traversed by the satellite within 8 s.

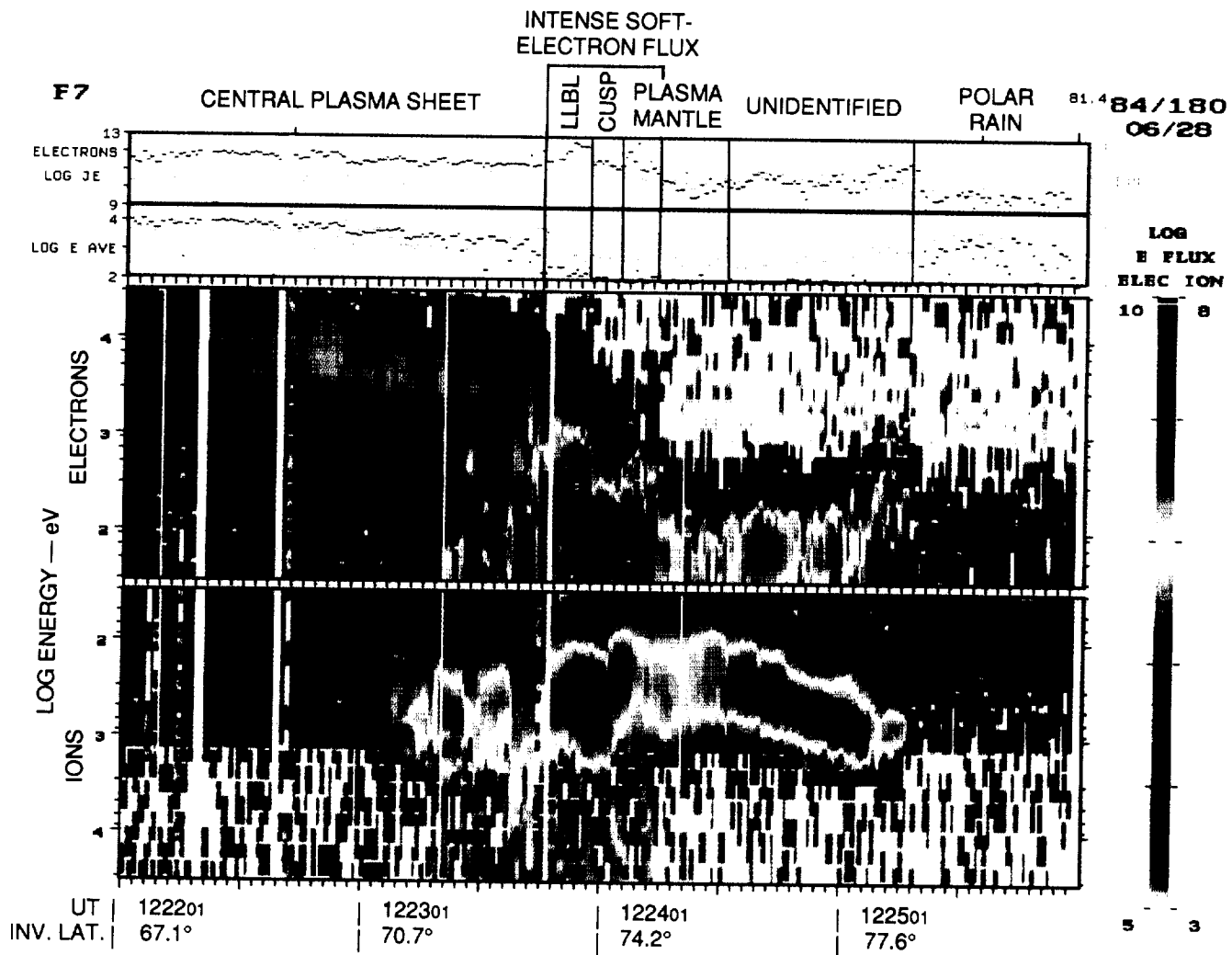


Plate 1. DMSF-F7 measurements of particle precipitation during a cusp pass over Sondrestrom on June 28, 1984, around 1224 UT. (Top) electron and ion band integrated energy flux and average energy; (middle and bottom) electron and ion energy flux spectrograms (30 eV to 30 keV) in $\text{eV cm}^{-2} \text{s}^{-1} \text{sr}^{-1} \text{eV}^{-1}$, with the ion ordinate reversed.

The identification of the magnetospheric cusp from particle measurements on low altitude and mid altitude spacecraft relies on ion and electron flux properties [Newell and Meng, 1989; Kremser and Lundin, 1990]. Plate 1 shows that the intensity of the electron energy flux in the cusp and magnetospheric boundary layers (LLBL and PM) was between one and two orders of magnitude higher than the ion energy flux. Therefore, the ionospheric effects of cusp-like precipitation that we expect to observe are caused mainly by the electron flux, and the contribution of the ion flux to variations in plasma density and temperature is deemed insignificant. In Plate 1, we notice a region of intense low-energy (less than 500 eV) electron flux, which extends from the equatorward edge of the LLBL (at 73.2° invariant latitude) across the cusp and a part of the PM, up to 75.1° invariant latitude. The intensity of the electron flux is even lower in the cusp proper than in the adjacent LLBL and PM regions, and the average electron energy is slightly higher in the LLBL than in the cusp and PM.

Because we expect the radar to be sensitive to the ionospheric signature of the electron precipitation only, we treat this entire region of intense soft-electron precipitation as a single region and consider it characteristic of magnetosheathlike particle precipitation. In any case, the limited spatial resolution of the radar observations would hamper the exact identification of the boundaries between LLBL, cusp, and PM.

The geographic setting of the event is shown in Figure 1. The Sondrestrom radar location is marked by a full diamond labeled SSF. The line through the radar indicates the orientation of the elevation scan plane, the heavy section represents the scan trace at 120-km altitude, and its thin extension the scan trace at 350-km altitude. Dotted lines indicate E region (120-km altitude) contours of equal invariant latitudes. The DMSF-F7 trajectory mapped down to 120-km altitude is indicated by a thin line with diamond markers separating CPS, LLBL, cusp (indicated by the heavy segment), PM, the unidentified interval, and PR. The hatched

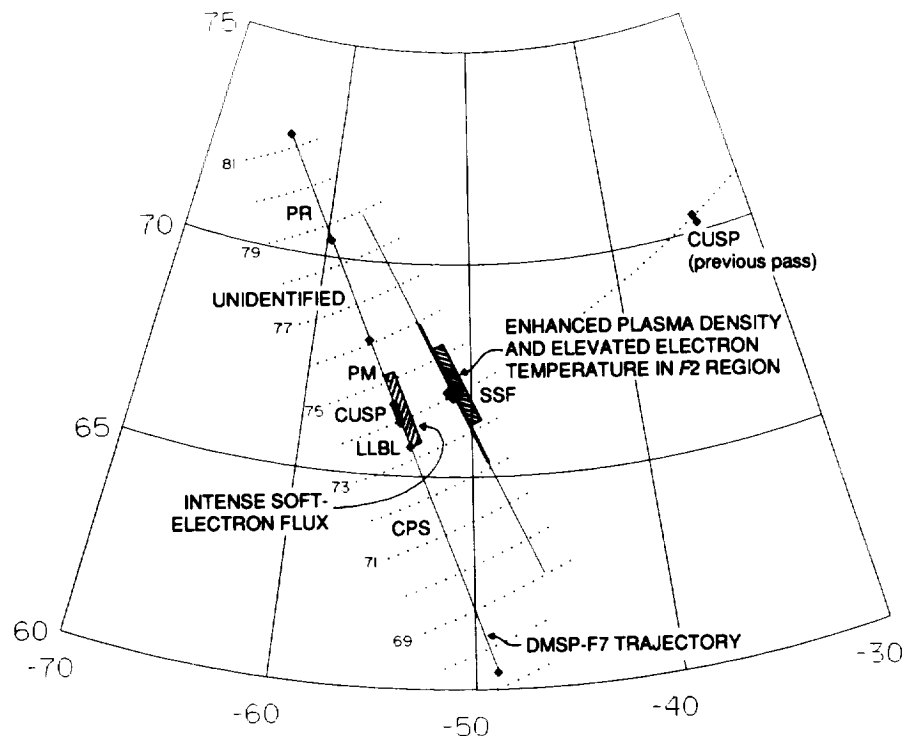


Figure 1. The DMSF-F7 pass of June 28, 1984, 1222–1226 UT, mapped down to 120-km altitude and projected on a geographic grid with dotted contours of equal invariant latitude. Also shown are the Sondrestrom radar location (diamond labeled SSF) with the antenna elevation scan trace at 120 km (thick) and 350 km (thin) and the location of the particle cusp during this and the previous satellite passes. The regions with intense soft-electron precipitation and increased *F2* region electron density and temperature are indicated by hatched segments.

segment spans the region of intense soft-electron precipitation, including LLBL, cusp, and the equatorward part of PM. No significant precipitation was measured beyond the equatorward and poleward end points of the satellite trajectory segment plotted here. The geometry of this event is such that the DMSF-F7 trajectory is approximately parallel to the radar elevation scan plane and perpendicular to the contours of constant invariant latitude.

A second heavy trace segment close to the right margin of Figure 1 indicates cusp precipitation observed by DMSF-F7 on its preceding pass, 102 min earlier. The satellite identified the cusp at 10 MLT between 73.6° and 73.9° invariant, that is, almost at the same invariant latitude as during the following pass which was closer to Sondrestrom. If we assume that no significant fluctuations of the particle cusp invariant latitude occurred between these two passes, we expect its ionospheric footprint to be approximately overhead of the radar at the time of the 1222–1226 UT satellite pass. In Figure 1, we have indicated by a hatched segment along the radar scan the interval where the radar detected enhanced electron density and elevated electron temperature in the *F2* region over the 1.5 hours following this satellite pass. The relevant radar observations (Figure 2) demonstrate that the equatorward and poleward boundaries of this particular ionospheric region are indeed found nearly at the same invariant latitudes

as the boundaries of the intense soft-electron precipitation observed by DMSF-F7.

In Figure 2 we show the plasma density, the electron temperature, and the ion temperature, inferred from radar elevation scans, as stacks of clock dial plots in 50-km altitude steps. Time runs counterclockwise around the circle, with 1400 UT (approximately 12 MLT) at the top; invariant latitude covers the range 68° to 80° from outward to inward. At each altitude, the DMSF-F7 pass is marked by a radial line with a heavy segment, which corresponds to the intense soft-electron precipitation region. The plasma density and temperature scaling bars change with altitude. The numbers printed to the right of the clock dials correspond to the fixed altitudes printed on the left. In each pair of scale numbers, the smaller number marks the upper limit of the blank bin; all densities or temperatures below this level and possible data gaps appear blank. The higher number marks the lower limit of the darkest bin; all densities and temperatures exceeding this level appear black. Note that the data plotted in Figure 2, and also those plotted in Figure 3, do not represent a snapshot of the ionosphere, but rather a combination of spatial variation and temporal evolution sampled by the radar as it rotates, fixed to the Earth, under the high-latitude ionosphere. Because of the interpolating software used to generate Figure 2, this figure might give the impression of a better resolution than is actually available:

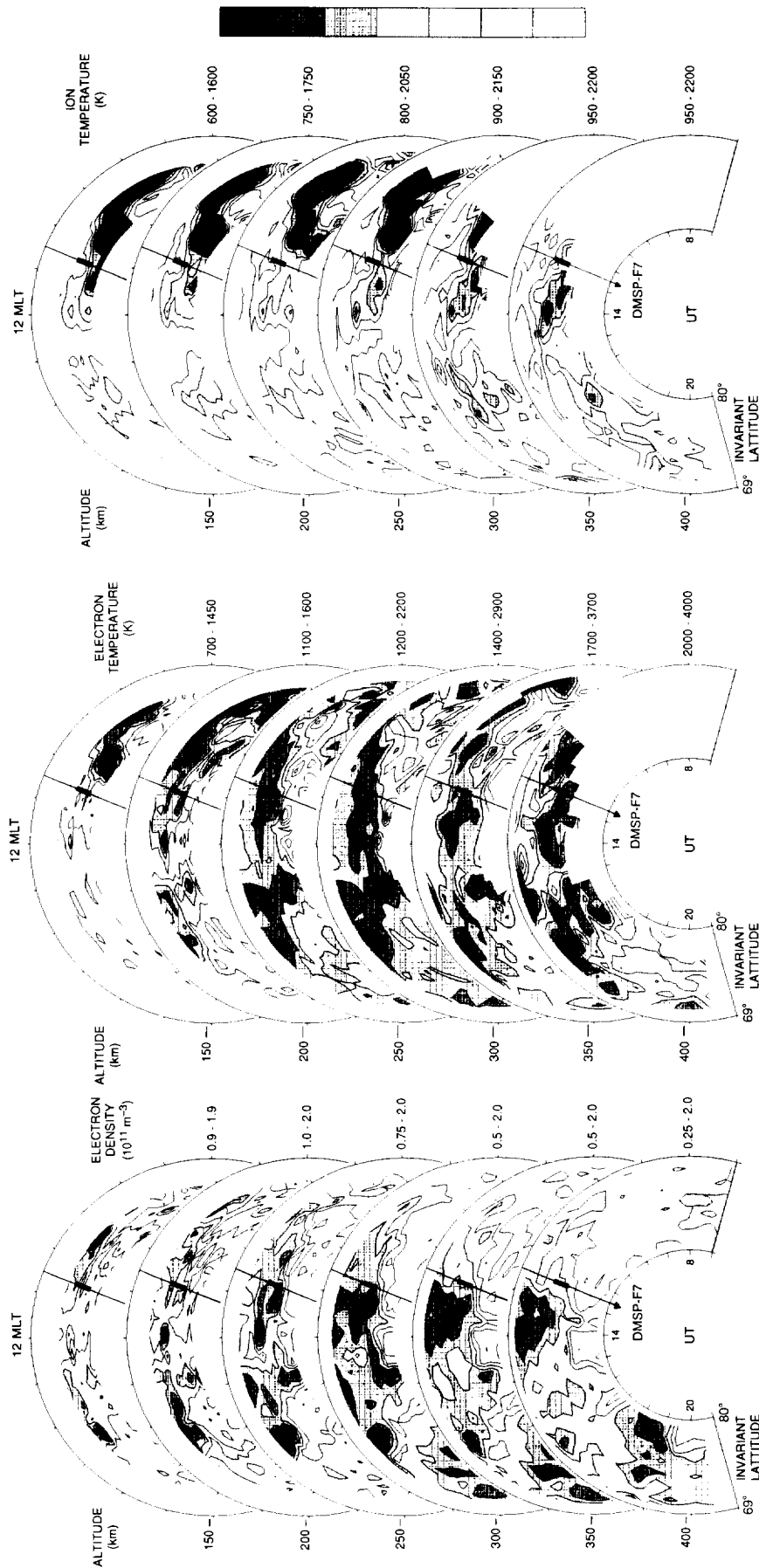


Figure 2. Plasma density, electron temperature, and ion temperature in clock dial stacks with 50-km altitude separation. Time runs counterclockwise, invariant latitude covers the range from 69° to 80° from outside to inside. Note that the gray scale varies with altitude, as indicated by the pair of numbers written on the same line as the altitude. The heavy segment on the DMS-P-F7 trajectory (between 1200 and 1300 UT) marks the region of intense soft-electron precipitation.

The antenna cycle time limited the temporal resolution (at a given latitude) to some 25 min. Specifically, the DMSP-F7 pass fell exactly between two elevation scans; thus ionospheric plasma-density and temperature profiles are available only some 10 min before and after the pass.

At 150- and 200-km altitude, we notice scattered patches of enhanced electron density in the morning prior to the satellite pass and also in the afternoon. They are accompanied by elevated electron and ion temperatures. A careful examination shows that the elevated temperatures appear close to, but not coincident with, the increased plasma density. A band of enhanced plasma density appears at 250- and 300-km altitude at the same invariant latitudes where DMSP-F7 observed intense soft-electron precipitation. This band begins with the DMSP-F7 pass and extends over about 1.5 hours. Because of the 20-min gap between two consecutive radar scans, it is more accurate to say that the radar did not observe enhanced plasma density in the scan before the pass but observed it in the scan following the pass. (This applies also to the temperatures, discussed below.) The band of enhanced plasma density is about 2° wide in latitude. It is most pronounced at 250- and 300-km altitude and fades at higher altitudes. The enhanced plasma density coincides with elevated electron temperature. This is barely noticeable at 200-km altitude but becomes more prominent with each upward altitude step. A slight ion temperature increase is seen only from 300 km upward and mainly at the poleward edge of the soft-electron flux region. At 400-km altitude, the ion temperature seems to coincide with the soft-electron precipitation, but unfortunately reliable radar data are scarce. At 350- and 400-km altitude, a plasma tongue in the equatorward part of the radar field of view between 1230 and 1430 UT gradually assumes dominance. It is not accompanied by increased electron and ion temperatures. This high-altitude plasma tongue is most likely the poleward tip of a region of enhanced dayside ionization generated by solar radiation that was subsequently advected into the polar cap. We do not show data from above 400 km because the radar return signals were weak and the temperature measurements uncertain.

The radar data show that enhanced electron density, elevated electron temperature and slightly elevated ion temperature coincide only in a 2° -wide area along 74° invariant latitude, between 1230 and 1400 UT. It is most clearly seen in the 300-km altitude data. This interval coincides with the latitude range where DMSP-F7 measured intense soft-electron precipitation, and we suggest that these particular ionospheric plasma properties are the result of such precipitation. Further down, we show that this signature agrees with predictions from an ionospheric model.

The radar observations of the plasma convection are plotted in Figure 3, also in a clock dial stack. The upper section shows results from the multiposition part of the antenna cycle, whereby it is assumed that drift magnitude and orientation with respect to the magnetic

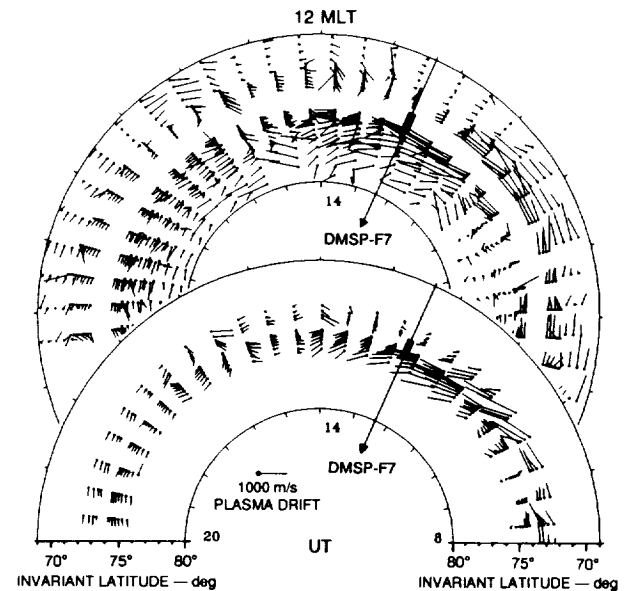


Figure 3. Plasma flow pattern inferred from (top) multiple fixed antenna positions and (bottom) elevation scans of the Sondrestrom radar. Clock dial representation with DMSP pass as indicated in Figure 2.

field are the same at both positions of a fixed position pair. The drift measured parallel to the geomagnetic field was used to construct the full velocity vector. The lower section shows the drift inferred from the elevation scans using a method developed by *de la Beaujardière et al.* [1977]. In this method, *E* and *F* region line-of-sight ion velocities are merged, taking the different altitude dependencies of the Pedersen and Hall mobilities into account. Fixed-position radar measurements use only *F* region data and cover a wider latitude range than the elevation scan measurements, which rely on *E* and *F* region data. The drift patterns obtained with the two different methods are very similar in the latitude range where they overlap, lending confidence to the convection pattern derived.

The hours around the DMSP-F7 pass are characterized by eastward (sunward) plasma drift averaging near 1 km/s poleward of the radar while much smaller velocities are found equatorward of the radar. We notice a poleward turning of the plasma drift from 1230 UT onward in the equatorward section of the convection pattern, which we associate with the conjunction of the morning and afternoon convection cells. No IMF data are available for the time after 1030 UT; however, before 1030 UT, the B_y and B_z components of the IMF were negative (-9 and -4 nT, respectively) and remained fairly constant for many hours. We suspect that these IMF conditions prevailed after 1030 UT because the cusp was observed at a relatively low invariant latitude and early local time. This is more typical for a situation where B_y and B_z are both negative than for any other combination of the B_y and B_z directions [Newell et al., 1989].

The radar plasma flow measurements contain a gap (radar blind spot) in the vicinity of the radar loca-

tion (74° invariant latitude) and thus do not cover, on a small scale, the soft-electron flux region. Therefore we cannot deduce whether the convection reversal was within the cusp or at its equatorward or poleward boundary. In a steady state situation, it is usually assumed that the cleft (which maps to the LLBL) [cf. *Vasyliunas*, 1979] lies on closed and the cusp on open field lines and that the boundary between closed and open field lines coincides with the convection reversal. *Foster et al.* [1989] indeed place the cusp/cleft boundary at the same latitude as the convection reversal. *Cowley et al.* [1991] argue that the boundary between open and closed field lines lies poleward of the convection reversal, because of momentum transfer by viscous interaction at the magnetopause. It is also sometimes assumed that the cusp lies within the high-latitude convection throat, but *Lockwood* [1991] notes that, owing to the IMF B_y dependence of the convection pattern, the throat is not a good indicator of the cusp position. We have examined several cases in which the ionospheric footprint of the particle cusp was monitored by the Sondrestrom radar and have found that neither the convection reversal nor the throat clearly determine the position of the cusp [*Watermann et al.*, 1992].

Examination of the ambient electron energy balance supports our view that we observed a signature of soft particle precipitation. Enhanced F region electron density, if not locally produced, corresponds to a low electron-loss rate. This is typical for weak electric fields [e.g., *Schunk et al.*, 1975], unlike that measured within the poleward section of the soft-particle precipitation region. We also find an increase of the F region electron energy loss rate within the particle cusp. We computed the rate of energy loss from electrons to ions and neutrals [*Kofman and Wickwar*, 1984] for different antenna positions of the multiposition part of that radar cycle that coincided with the DMSP-F7 pass. The total electron energy loss rate depends on neutral and charged particle density and neutral composition, as well as ion, electron, and neutral temperatures. Figure 4 shows this loss rate from observations in five radar positions close to the time of the DMSP pass. When the radar beam was parallel to the magnetic field (symbol F) and intersected the area of increased $F2$ layer electron density and temperature, the electron energy loss rate was significantly larger than on each of the two closest antenna position pairs, one pair looking poleward (P) and the other equatorward (E). Because of the lower antenna elevation, the equatorward and poleward pointing radar beams remained within the field lines threaded by intense soft-electron precipitation only up to some 170-km altitude. The coincidence of a high electron energy loss rate with high plasma density and elevated electron temperature in the F region strongly supports our view that the radar data show the ionospheric effects of locally confined intense soft-particle precipitation and the subsequent energy loss of the ambient electrons to the ions and neutrals, as described by *Schunk and Nagy* [1978].

We have not plotted data from the other two days of

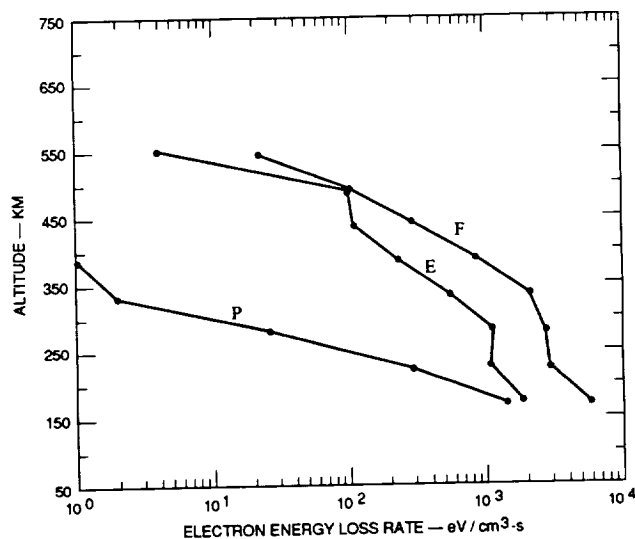


Figure 4. Electron energy loss rates (in eV cm^{-3}) obtained from radar measurements at three fixed antenna positions around the time of the DMSP-F7 cusp pass. P, antenna pointing poleward; F, field-aligned; E, equatorward. In the field-aligned position, the radar beam intersects the high-density, high-temperature F region plasma and shows the highest energy-loss rate.

the World Day campaign, June 26 and 27. On June 26 the particle cusp was detected by DMSP-F7 poleward of the radar field of view, and it was not at all detected on June 27. Examination of the radar data from June 26 to 27 did not reveal signatures like those observed on June 28, which we discussed above. Instead, on June 26 and 27 the daytime plasma density distributions showed a smooth slowly varying pattern, representative for a diurnal variation as expected from a stable sunlit ionosphere.

The magnetic perturbation along the DMSP-F7 trajectory was derived from DMSP-F7 magnetometer observations following the procedure of *Rich et al.* [1991]. Three-second averages of the horizontal perturbation vector (which is approximately perpendicular to the geomagnetic main field at this high latitude with 80° dip angle) are plotted in Figure 5. The magnetospheric regions associated with the observed particle fluxes are indicated, and the intense soft-electron precipitation interval is marked by a thick bar. In the CPS regime, a northwestward magnetic field perturbation prevails. Within the LLBL, its amplitude and orientation change considerably toward a larger and mainly west-southwest oriented magnetic perturbation field. From thereon throughout the cusp, the PM and the unidentified region the orientation changes very little. The amplitude, however, grows even larger within the PM to reach its maximum near the poleward edge of the intense soft-electron flux interval, and then drops gradually to less than 100 nT in the polar rain region. Note that significant variations of either amplitude or orientation of the magnetic perturbation and its maximum amplitude occur within the different particle regions but not at their

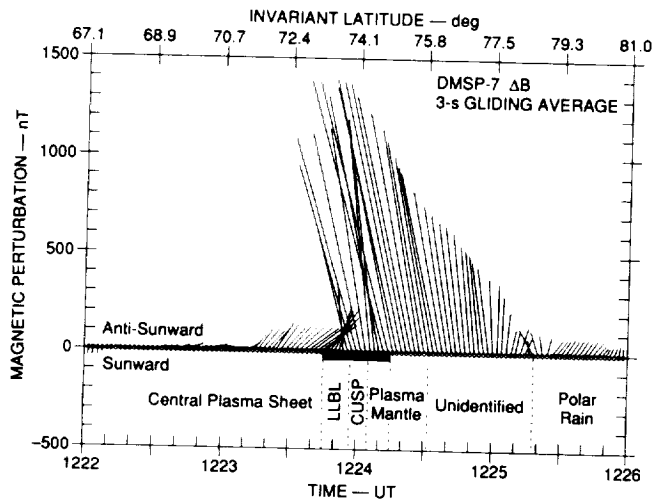


Figure 5. Horizontal magnetic perturbation vectors inferred from DMSP-F7 magnetometer measurements. The footprints of magnetospheric regions are indicated, the interval of intense soft-electron flux (covering LLBL, cusp, and the equatorward part of the PM) is marked by a thick line.

boundaries, with the only exception of the equatorward boundary of the polar rain. *De la Beaujardière et al.* [1993], who analyzed eleven DMSP passes through the dayside auroral zone, concluded that current intensifications (identified by sharp gradients in the magnetic field amplitude) and transitions between upward and downward currents (identified by the maximum amplitude of the magnetic perturbation) occur in general within the different particle regions and not at their boundaries. These particle and magnetic field measurements, made simultaneously on the same spacecraft, demonstrate that the distribution of field-aligned currents does not in general allow the determination of the footprints of magnetospheric boundary regions and specifically the particle cusp.

We finish this section by summarizing the pertinent observational features from the June 28, 1984, event, which are sketched in Figure 6. Between 1230 and 1400 UT (approximately 10.5 to 12 MLT, that is, close to magnetic noon) the radar observed an ionospheric patch some 2° wide in invariant latitude which was characterized by enhanced F_2 region plasma density, elevated electron temperature, slightly elevated ion temperature, and a high electron-energy-loss rate. The plasma temperature elevations dominate at the higher altitudes. The dark area shows the region where the Sondrestrom radar measured electron density and temperature in excess of $2 \times 10^{11} \text{ m}^{-3}$ and 2800 K, respectively, at 300-km altitude. These thresholds are somewhat arbitrarily, the black area would shrink or expand when the thresholds are increased or decreased, respectively. The box on the DMSP-F7 trace indicates the interval where intense soft-electron precipitation was measured. The arrows delineate the plasma flow pattern. Because of the predominantly zonal plasma flow and the very small poleward flow components, it seems

unlikely that the plasma patch constitutes remnant ionization from solar radiation that had drifted poleward into the radar field of view. If the patch were associated with the flow shear, it should appear as cool as the background plasma and also extend further along the flow reversal line into the afternoon sector. We suggest to interpret the radar observations as an ionospheric signature of magnetosheathlike plasma precipitation.

We have discussed the radar data mainly in the context of soft-electron precipitation rather than LLBL, cusp, and PM precipitation. The reason is that we are not able to distinguish between LLBL, cusp, and PM solely from the radar measurements. In this event, the electron fluxes in these regions were too similar, and the ionosphere is not very sensitive to the ion precipitation which was of low intensity. We have examined other cases with sharp electron precipitation boundaries between, for instance, the ring current region and the cusp, and we find that the gradients of the ionospheric F region plasma density and temperature are not very sharp, probably because of the smearing effect of horizontal plasma convection.

Model Predictions

We have used an auroral model [*Lummerzheim*, 1987] to predict the ionospheric plasma density and temperature distribution during this event. The model in its currently available one-dimensional version does not take into consideration horizontal diffusion and convection. It consists of two major parts, which are differentiated by the characteristic timescales of the included processes: The first part deals with transport of energetic particles and resulting excitation and ionization processes; the second part covers the thermospheric chemistry and diffusive transport. The major ionization sources used in this model include electron precipitation, solar EUV radiation, and photoelectrons.

Input parameters to the model are provided by specifying an electron flux spectrum above the ionosphere (but below the auroral acceleration zone), a thermosphere model (at present, the MSIS-90 model, see *Hedin*

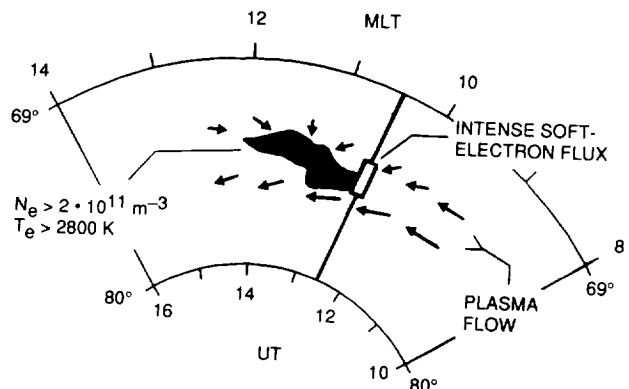


Figure 6. Simplified sketch of incoherent scatter radar observations during the DMSP-F7 cusp pass on June 28, 1984.

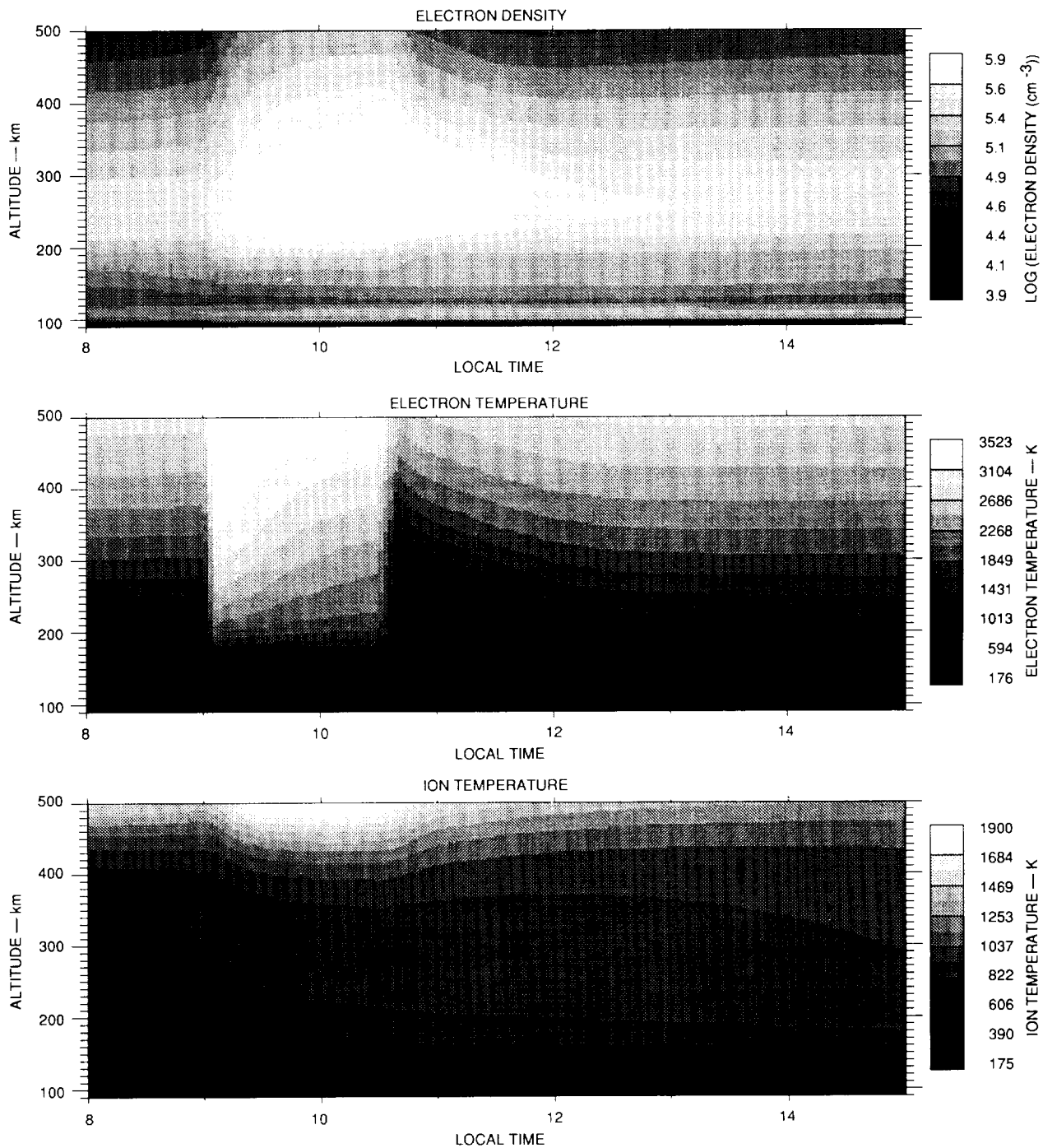


Figure 7. Model calculations of ionospheric plasma density and electron and ion temperature variations with local time. Soft-particle precipitation as measured by DMSP-F7 during the cusp crossing on June 28, 1984, 1224 UT, is effective between 9.0 and 10.5 local time. The model is one-dimensional, that is, no plasma convection is included.

[1991]), solar activity (i.e., the 10.7-cm flux), magnetic activity (the A_p index), and the day of the year and solar local time. The ionization rates obtained serve as input to the ion chemistry part, which is built on the reaction rates given in the appendix of *Rees* [1989]. Finally, the electron and ion energy equations are solved. The model then predicts time-dependent vertical profiles of the plasma density, ion composition, and electron and ion temperatures, among other parameters.

This model allows for pitch angle dependent electron precipitation, but we cannot make use of this detail, because the DMSP spectrometers point always vertically upward and make only one-directional flux measurements. However, this does not pose a significant problem in the cusp because Viking measurements of pitch angle resolved cusp electron precipitation have shown that the cusp electron flux is virtually isotropic [*Aparicio et al.*, 1991]. Therefore we feel it is justified to as-

sume isotropy for the cusp electron spectra observed on DMSP-F7. Isotropy is not normally found in the LLBL precipitation [Lundin, 1988], therefore the DMSP particle measurements in the LLBL were not used in the model calculations.

When we applied the model to our event, we reduced the atomic oxygen density obtained from the MSIS standard atmosphere by a factor of 2. Such a reduction factor is perhaps justified by reports that the MSIS model tends to overestimate the atomic oxygen abundance in the *E* region during times of auroral precipitation [Hecht and Strickland, 1988; Lummerzheim et al., 1990]. This modification led to a better agreement between radar observations and model predictions. As input spectrum to the model, we used an average over the spectra observed by DMSP-F7 in the interval labeled 'cusp' in Plate 1 and Figures 1 and 5. Because DMSP-F7 measured the electron flux only above 30 eV energy we had to make assumptions about the extrapolation of the spectrum to lower energies. Test runs with different extrapolations have shown that the modeled plasma density distribution is virtually independent of the electron flux intensity below 30 eV, but that the plasma temperature above some 300-km altitude depends noticeably on the suprathermal electron flux. The temperature distributions that we obtained are therefore only qualitatively valid above 300 km. In our simulation, we assumed that a corotating station entered a region of constant soft-electron precipitation at 0900 solar local time (SLT), equivalent to 1224 UT (i.e., the time of the DMSP-F7 pass over Sondrestrom), and left it 1.5 hours later, at 1030 SLT (1354 UT).

Figure 7 shows in an altitude versus SLT frame the ionospheric plasma density and temperature variations predicted by the auroral model. The upper panel shows that the *F* region plasma density increases steadily during the precipitation period. More detailed examination of the model output indicates that the peak plasma density approaches nearly saturation toward the end of the precipitation. The plasma density enhancement is significant only above some 200-km altitude and reaches a peak of about 2.5 times the quiet pre-precipitation state. The electron temperature reacts immediately to the precipitation onset; it rises sharply and leads to a slow but steady rise of the scale height as long as the precipitation is sustained. This temperature effect is seen only at higher altitudes, above some 180 km, and becomes more pronounced with increasing altitude. For an observer at a fixed altitude, the electron temperature shoots up at the precipitation onset, tends to recover partly during the ongoing precipitation, and drops when precipitation ceases, but remains above the pre-precipitation level. Two and a half hours after the precipitation is shut off, the electron density and temperature resume their normal (solar radiation controlled) level. The ion temperature reacts more slowly, the temperature increase is marginal below 400 km and significant only at higher altitudes.

The characteristic features of the model simulation include a gradual increase of the *F* region plasma den-

sity to a maximum in the 200- to 300-km altitude range, an immediate increase of the electron temperature at all *F* region altitudes, but most pronounced at altitudes higher than the *F* region density peak, and a slight increase of the ion temperature which is delayed in time and becomes significant only at the highest altitudes.

For comparison, we have run the model with an input electron spectrum as measured by DMSP-F7 around 1222:50 UT, that is, at the time of the most intense CPS precipitation (see Plate 1). In that case, the plasma density will be noticeably enhanced only below some 130 km but not in the *F* region, and we find a very small elevation in the electron temperature from some 150 km upward, and no change in the ion temperature. The plasma density and temperature predictions shown in Figure 7 are thus clearly indicative of soft-electron precipitation.

Discussion and Conclusions

We have demonstrated that the ionospheric footprint of soft-electron precipitation can be identified from ground-based incoherent scatter radar observations. In the event discussed here, the DMSP-F7 spacecraft traversed a region of intense soft electron flux. Its intensity and characteristic energy suggest that the particles are directly or indirectly of magnetosheath origin. The region included the LLBL, the cusp, and the equatorward section of the PM. The distinction between these regions is based mainly on the satellite observations of the ion flux. This is consistent with *Johnstone* [1985], who claims that cusp and PM electrons are magnetosheathlike and therefore indistinguishable while the respective proton energy distributions differ. Because the intensity of the ion-energy flux is an order of magnitude or more below that of the electron flux, we do not expect that we can distinguish these three regions by their ionospheric signatures. Radar observations of plasma density and temperature show indeed a correlation with the intense soft-electron flux region, but the radar measurements do not allow to resolve a further subdivision, because of the similar electron spectra in these three regions and the limited resolution of the radar data.

The agreement between model results and radar observations of *F* region plasma density and temperature distributions, although not fully satisfactorily, lends confidence to the ionospheric model and to our interpretation of the radar observations. The largest discrepancy appears in the plasma density distribution: The *F* region peak density measured with the radar reaches only about $3 \times 10^{11} \text{ m}^{-3}$ within the precipitation region, and the model predicts almost $8 \times 10^{11} \text{ m}^{-3}$. The agreement between the measured and modeled electron temperatures is much better: radar data from 300-km altitude, just above the *F* region density peak, show an electron temperature maximum of some 3000 K, while the model gives at this altitude 2900 K soon after the precipitation onset and 2300 K after the precipitation has lasted for more than one hour. Model calcula-

tions and radar observations of ion temperatures near the F region peak show little dependence on presence or absence of precipitation. It is interesting to note that the differences between measurements and model predictions are systematic. Before, during, and after the precipitation, the modeled plasma density is higher than the measured, and the modeled electron and ion temperatures are lower than the measured.

Part of the discrepancy is probably explained by the model design. Because the model is only one-dimensional, no mechanism for plasma depletion by horizontal transport is included. The specific geophysical conditions on June 28 may have been unusual, as a comparison between measurements from this and the previous day (June 27) reveals. On June 27, DMSP-F7 measured electron precipitation of about 1-keV average energy and $8 \times 10^{-3} \text{ J m}^{-2} \text{ s}^{-1}$ average integrated energy flux between 72° and 76° invariant latitude. On 28 June, the corresponding numbers for the cusp are 100–150 eV average energy and $1.6 \times 10^{-3} \text{ J m}^{-2} \text{ s}^{-1}$ energy flux. On June 27, electron precipitation had therefore much less effect on the F region plasma above the radar site than it had on June 28. However, on June 27, the F region peak density measured on the field line through the radar site hovered around $2.5 \times 10^{11} \text{ m}^{-3}$ during several hours from late morning into the afternoon, compared to $1.7 \times 10^{11} \text{ m}^{-3}$ (outside the cusp region) on June 28. On June 27, the Kp index did not exceed 20 and the AE value stayed below 200 nT during the daytime hours while on June 28 the Kp index reached 40 and AE some 1000 nT. Obviously, on June 28 there was significantly higher geomagnetic and electrojet activity, consistent with the observed large plasma velocities on June 28 (see Figure 3) which at times exceeded 1000 m/s in the poleward part of the radar field of view. According to Schunk *et al.* [1975], equations (16)–(22), a 1000-m/s plasma drift (or, equivalently, a 50-mV/m electric field) would increase the effective F region ion temperature by about 800 K over the neutral temperature. Such a temperature increase results in higher O^+ reaction rates and consequently reduced plasma density because the molecular ions recombine much faster than atomic oxygen. Our auroral model cannot account for the effects of the large electric field. The high geomagnetic and electrojet activity on June 28 therefore provides a possible explanation for the observed discrepancy between measurements and model predictions.

This event and a few others that we examined demonstrate that an incoherent scatter radar can identify regions of soft-particle precipitation by their F region signatures. We assume that these regions are threaded by open field lines connected to the exterior cusp and to magnetospheric boundary layers such as the LLBL (at least sometimes) and the PM. The open field lines allow magnetosheath plasma a more or less direct access to ionospheric altitudes. The events we have analysed so far suggest that a subdivision into LLBL, cusp, and PM, based solely on incoherent scatter radar observations, is often impossible. Whether the method can be refined so that it will in general be possible to distin-

guish the footprint of the particle cusp from the LLBL and PM is still an open question. One of the principal difficulties concerns the role of the ion precipitation, an important indicator of magnetospheric regions. Hardy *et al.* [1989] have shown that the ion energy flux along the noon-midnight meridian is on the average an order of magnitude below the electron energy flux at all levels of geomagnetic activity. While spaceborne particle spectrometers can determine the characteristics of the ion precipitation irrespective of electron precipitation, the ionospheric response (ionization and plasma thermalization) is dominated by the more intense electron precipitation. In this particular event, we also faced the problem of the limited spatial resolution of the radar measurements. From an analysis of Viking data, Aparicio *et al.* [1991] found the average width of the statistical cusp (including cusp proper, boundary cusp and mantle cusp) to be 2° in magnetic latitude, while Newell and Meng [1988, 1992] determined from DMSP-F7 and -F9 observations an average (but highly variable) cusp width of about 1° . In future experiments, we will therefore operate the Sondrestrom radar in a mode that provides better spatial resolution than was achieved in previously performed experiments.

A question remains as to how the ionospheric electrostatic potential distribution (or equivalently the plasma convection pattern) is related to the particle cusp. The example discussed here as well as some other cases that we have examined indicate that measurements of the F region plasma density and temperature distributions have the potential of being a better cusp identifier than measurements of the plasma convection. We also emphasize that the magnetic perturbation field measured by DMSP-F7 does not exhibit significant changes in amplitude or orientation that coincide with the equatorward and poleward boundaries of the particle cusp. Because the magnetic perturbation conveys information about the field-aligned currents, we believe that field-aligned currents cannot serve as a cusp identifier either.

We acknowledge that analysis of a few individual events is not sufficient to determine how and under which conditions the particle cusp or more generally a flux tube filled with magnetosheath plasma can reliably be identified from incoherent scatter radar measurements. We plan to examine more coincident radar and spacecraft data to determine if particular geophysical conditions facilitate observation of such signatures with the radar.

Acknowledgments. This work was supported by the National Science Foundation through the Cooperative Agreement ATM-8822560 with SRI International and through Grants ATM-9112680 to SRI, ATM-9022197 to UAF, and ATM-9108193 to APL/JHU. NASA support was provided under contract NASW-4603 with SRI and Grant NAGW-3037 to UAF. Magnetic field line tracing and conversion of geographic coordinates to invariant latitude was performed using the IGRF model software supplied by the National Space Science Data Center (NSSDC)/World Data Center A for Rockets and Satellites.

The editor thanks M. J. Engebretson and J. M. Holt for their assistance in evaluating this paper.

References

- Aparicio, B., B. Thelin, and R. Lundin, The polar cusp from a particle point of view: A statistical study based on Viking data, *J. Geophys. Res.*, *96*, 14023, 1991.
- Baker, K.B., R.A. Greenwald, J.M. Ruohoniemi, J.R. Dudeney, M. Pinnock, P.T. Newell, M.E. Greenspan, and C.-I. Meng, Simultaneous HF-radar and DMSP observations of the cusp, *Geophys. Res. Lett.*, *17*, 1869, 1990.
- Bythrow, P.F., T.A. Potemra, R.E. Erlandson, L.J. Zanetti, and D.M. Klumpp, Birkeland currents and charged particles in the high-latitude prenoon region: A new interpretation, *J. Geophys. Res.*, *93*, 9791, 1988.
- Cowley, S.W.H., J.P. Morelli, and M. Lockwood, Dependence of convective flows and particle precipitation in the high-latitude dayside ionosphere on the X and Y components of the interplanetary magnetic field, *J. Geophys. Res.*, *96*, 5557, 1991.
- de la Beaujardière, O., R. Vondrak, and M. Baron, Radar observations of electric fields and currents associated with auroral arcs, *J. Geophys. Res.*, *82*, 5051, 1977.
- de la Beaujardière, O., J. Watermann, P. Newell, and F. Rich, Relationship between Birkeland current regions, particle precipitation, and electric fields, *J. Geophys. Res.*, *98*, 7711, 1993.
- Engebretson, M.J., B.J. Anderson, L.J. Cahill, Jr., R.L. Arnoldy, T.J. Rosenberg, D.L. Carpenter, W.B. Gail, and R.H. Eather, Ionospheric signatures of cusp latitude Pc 3 pulsations, *J. Geophys. Res.*, *95*, 2447, 1990.
- Engebretson, M.J., C.-I. Meng, R.L. Arnoldy, and L.J. Cahill, Jr., Pc 3 pulsations observed near the polar cusp, *J. Geophys. Res.*, *91*, 8909, 1986.
- Foster, J.C., H.-C. Yeh, J.M. Holt, and D.S. Evans, Two-dimensional mapping of dayside convection, in *Electromagnetic Coupling in the Polar Clefts and Caps*, edited by P. E. Sandholt and A. Egeland, p. 115, Kluwer, Norwell, Mass., 1989.
- Hardy, D.A., L.K. Schmitt, M.S. Gussenhoven, F.J. Marshall, H.C. Yeh, T.L. Shumaker, A. Hube, and J. Pantazis, Precipitating electron and ion detectors (SSJ/4) for the block 5D/flights 6-10 DMSP satellites: Calibration and data presentation, *Rep. AFGL-TR-84-0317*, Air Force Geophys. Lab., Hanscom Air Force Base, Mass., 1984.
- Hardy, D.A., M.S. Gussenhoven, and D. Brautigam, A statistical model of auroral ion precipitation, *J. Geophys. Res.*, *94*, 370, 1989.
- Haerendel, G., G. Paschmann, N. Sckopke, H. Rosenbauer, and P.C. Hedgecock, The frontside boundary layer of the magnetosphere and the problem of reconnection, *J. Geophys. Res.*, *83*, 3195, 1978.
- Hecht, J.H., and D.J. Strickland, Measurements of E region atomic oxygen densities deduced from permitted optical auroral emissions and from incoherent scatter radar data (abstract), *Eos Trans. AGU*, *69*, 1346, 1988.
- Hedin, A.E., Extension of the MSIS thermosphere model into the middle and lower atmosphere, *J. Geophys. Res.*, *96*, 1159, 1991.
- Johnstone, A.D., Electron injection in the polar cusp, in *The Polar Cusp*, edited by J. A. Holtet and A. Egeland, p. 47, D. Reidel, Norwell, Mass., 1985.
- Kelly, J.D., Sondrestrom radar—Initial results, *Geophys. Res. Lett.*, *10*, 1112, 1983.
- Kofman, V., and V.B. Wickwar, Very high electron temperatures in the daytime F region at Sondrestrom, *Geophys. Res. Lett.*, *11*, 919, 1984.
- Kremser, G., and R. Lundin, Average spatial distributions of energetic particles in the midaltitude cusp/cleft region observed by Viking, *J. Geophys. Res.*, *95*, 5753, 1990.
- Lockwood, M., Incoherent scatter radar measurements of the cusp, in *Proceedings of CLUSTER Workshop* (Eur. Space Agency Spec. Publ., ESA SP-330), 57, 1991.
- Lummerzheim, D., Electron transport and optical emissions in the aurora, Ph.D. thesis, Univ. of Alaska, Fairbanks, 1987.
- Lummerzheim, D., M.H. Rees, and G.J. Romick, The application of spectroscopic studies of the aurora to thermospheric neutral composition, *Planet. Space Sci.*, *38*, 67, 1990.
- Lundin, R., Acceleration/heating of plasma on auroral field lines: Preliminary results from the Viking satellite, *Ann. Geophys.*, *6*, 143, 1988.
- Lundin, R., Magnetopause boundary layers, *J. Geomag. Geoelectr.*, *43*, Suppl., 165, 1991.
- McEwen, D.J., Optical-particle characteristics of the polar cusp, in *The Polar Cusp*, edited by J. A. Holtet and A. Egeland, p. 193, D. Reidel, Norwell, Mass., 1985.
- McHarg, M.G., and J.V. Olson, Correlated optical and ULF magnetic observations of the winter cusp-boundary layer system, *Geophys. Res. Lett.*, *19*, 817, 1992.
- Newell, P.T., and C.-I. Meng, The cusp and the cleft/boundary layer: Low-altitude identification and statistical local time variation, *J. Geophys. Res.*, *93*, 14549, 1988.
- Newell, P.T., and C.-I. Meng, On quantifying the distinctions between the cusp and the cleft/LLBL, in *Electromagnetic Coupling in the Polar Clefts and Caps*, edited by P. E. Sandholt and A. Egeland, p. 87, Kluwer, Norwell, Mass., 1989.
- Newell, P.T., and C.-I. Meng, Mapping the dayside ionosphere to the magnetosphere according to particle precipitation characteristics, *Geophys. Res. Lett.*, *19*, 609, 1992.
- Newell, P.T., C.-I. Meng, D.G. Sibeck, and R. Lepping, Some low-altitude cusp dependencies on the interplanetary magnetic field, *J. Geophys. Res.*, *94*, 8921, 1989.
- Olson, J.V., ULF signatures of the polar cusp, *J. Geophys. Res.*, *91*, 10055, 1986.
- Rees, M.H., *Physics and Chemistry of the Upper Atmosphere*, Cambridge University Press, New York, 1989.
- Rich, F.J., M.S. Gussenhoven, D.A. Hardy, and E. Holeman, Average height-integrated Joule heating rates and magnetic deflection vectors due to field-aligned currents during sunspot minimum, *J. Atmos. Terr. Phys.*, *53*, 293, 1991.
- Sandholt, P.E., A. Egeland, J.A. Holtet, B. Lybakk, K. Svenes, and S. Åsheim, Large- and small-scale dynamics of the polar cusp region, in *The Polar Cusp*, edited by J. A. Holtet and A. Egeland, p. 163, D. Reidel, Norwell, Mass., 1985.
- Schunk, R.W., and A.F. Nagy, Electron temperatures in the F region of the ionosphere: Theory and observations, *Rev. Geophys. Space Phys.*, *16*, 355, 1978.
- Schunk, R.W., W.J. Raitt, and P.M. Banks, Effect of electric fields on the daytime high-latitude E and F regions, *J. Geophys. Res.*, *80*, 3121, 1975.
- Sivjee, G.G., The effects of magnetosheath electrons on charge exchange, radiation trapping and other atomic and molecular processes in the mid-day polar cusp thermosphere, in *The Polar Cusp*, edited by J. A. Holtet and A. Egeland, p. 111, D. Reidel, Norwell, Mass., 1985.
- Vasyliunas, V.M., Interaction between the magnetospheric boundary layers and the ionosphere, in *Magnetospheric Boundary Layers*, edited by B. Battrock (Eur. Space Agency Spec. Publ., ESA SP-148), 87, 1979.
- Watermann, J., O. de la Beaujardière, and P.T. Newell, Incoherent scatter radar observations of ionospheric signatures of cusp-like electron precipitation, *J. Geomag. Geoelectr.*, *44*, 1195, 1992.

Wickwar, V.B., and W. Kofman, Dayside red auroras at very high latitudes: The importance of thermal excitation, *Geophys. Res. Lett.*, 11, 923, 1984.

O. de la Beaujardière, Geoscience and Engineering Center, SRI International, Menlo Park, CA 94025, U.S.A. (e-mail: odile@crvax.sri.com)

D. Lummerzheim, Geophysical Institute, University of Alaska, Fairbanks, AK 99701, U.S.A. (e-mail: lumm@loke.gi.alaska.edu)

P. T. Newell, Applied Physics Laboratory, Johns Hopkins University, Laurel, MD 20723, U.S.A. (e-mail: (SPAN) aplsp::newell)

F. J. Rich, Phillips Laboratory, Hanscom Air Force Base, Bedford, MA 01731, U.S.A. (e-mail: rich@plh.af.mil)

J. Watermann, NATO SACLANT Undersea Research Centre, Viale San Bartolomeo 400, I-19138 San Bartolomeo, La Spezia, Italy. (e-mail: waterman@saclantc.nato.int)

(Received February 19, 1993; revised July 1, 1993; accepted July 9, 1993.)

